MICROCOPY RESOLUTION TEST CHART
NATIONAL BUREAU

REPORT DOCUMENTATION PAGE		READ INSTRUCTIONS BEFORE COMPLETING FORM
1. REPORT NUMBER 13126.3-EL	2. GOVT ACCESSION NO.	3. RECIPIENT'S CATALOG NUMBER
4. TITLE (and Subtitle) Rays and Modes on Concave Surfaces		5. TYPE OF REPORT & PERIOD COVERED Final Report: 1 Jun 75 - 31 Aug 78
		6. PERFORMING ORG. REPORT NUMBER
7. AUTHOR(s) Leopold B. Felsen		8. CONTRACT OR GRANT NUMBER(s) DAHC04 75 G 0152
9. PERFORMING ORGANIZATION NAME AND ADDRESS Polytechnic Institute of New York Farmingdale, New York 11735		10. PROGRAM ELEMENT, PROJECT, TASK AREA & WORK UNIT NUMBERS
11. CONTROLLING OFFICE NAME AND ADDRESS U. S. Army Research Office P. O. Box 12211 Research Triangle Park, NC 27709		12. REPORT DATE Nov 78
		13. NUMBER OF PAGES 83
14. MONITORING AGENCY NAME & ADDRESS(if different from Controlling Office)		15. SECURITY CLASS. (of this report) Unclassified
		15a. DECLASSIFICATION/DOWNGRADING SCHEDULE

16. DISTRIBUTION STATEMENT (of this Report)

Approved for public release; distribution unlimited.

17. DISTRIBUTION STATEMENT (of the abstract entered in Block 20, if different from Report)

19. KEY WORDS (Continue on reverse side if necessary and identify by block number)

Rays
Modes
Electromagnetic Propagation
Concave Surfaces
Antennas
Ground Wave Propagation
Reflector Antennas
Conformal Antenna Arrays

20. ABSTRACT (Continue on reverse side if necessary and identify by block number)
The objective of the research program has been to gain an understanding of the electromagnetic propagation and diffraction properties of concave surfaces having radii of curvature large compared to the wavelength, with application to ground wave propagation, large reflector antennas, and mutually coupled conformal antenna arrays. This basic objective has been accomplished. When the program was initiated, there was only incomplete and non-conclusive information available on how the radiation, diffraction and guiding of fields is affected by a nearby

DD FORM 1473 EDITION OF 1 NOV 65 IS OBSOLETE

20. ABSTRACT CONTINUED

large-radius concave surface. It was recognized that neither a geometrical optics nor a whispering gallery mode representation is satisfactory for description of the field, and that a mixture of rays and modes, or a more complicated formulation involving a canonical integral analogous to the Fock integral for convex surfaces, may be the most effective. However, the foundations for these conjectures were lacking; accurate criteria for the appropriate combination of rays and modes were not at hand, nor were comprehensive numerical comparisons to assess the utility and quality of various field representations. Missing also were tractable results for the case when the observation point approaches the source or when the radius of curvature of a circular contour tends to infinity (infinite plane limit). This work has succeeded in establishing a sound analytical basis for any of the above-mentioned field formulations.

⑥ RAYS AND MODES ON CONCAVE SURFACES.

⑨ FINAL REPORT, 1 Jun 75 - 31 May 78,

⑩ LEOPOLD B. FELSEN

NOVEMBER 16, 1978

⑪ 16 Nov 78

U.S. ARMY RESEARCH OFFICE   ⑫ 90 P'

GRANT NO. DAHC-04-75-G-0152   ⑮ ✓

408 712

POLYTECHNIC INSTITUTE OF NEW YORK

⑱ ARO   ⑰ 13226.3-EL

APPROVED FOR PUBLIC RELEASE;
DISTRIBUTION UNLIMITED.

408 712

Summary.

The objective of the research program under Grant No. DAHC 04-75-G-0152, extending from 1 June 1975 to 31 May 1978, has been to gain an understanding of the electromagnetic propagation and diffraction properties of concave surfaces having radii of curvature large compared to the wavelength, with application to ground wave propagation, large reflector antennas, and mutually coupled conformal antenna arrays.

This basic objective has been accomplished. When the program was initiated, there was only incomplete and non-conclusive information available on how the radiation, diffraction and guiding of fields is affected by a nearby large-radius concave surface. It was recognized that neither a geometrical optics nor a whispering gallery mode representation is satisfactory for description of the field, and that a mixture of rays and modes, or a more complicated formulation involving a canonical integral analogous to the Fock integral for convex surfaces, may be the most effective. However, the foundations for these conjectures were lacking; accurate criteria for the appropriate combination of rays and modes were not at hand, nor were comprehensive numerical comparisons to assess the utility and quality of various field representations. Missing also were tractable results for the case when the observation point approaches the source or when the radius of curvature of a circular contour tends to infinity (infinite plane limit).

Our work has succeeded in establishing a sound analytical basis for any of the above-mentioned field formulations. Most important, we have shown that a mixture of ray-optical and whispering gallery mode fields alone, chosen in correct proportion, is indeed capable of providing accurate field values on the concave surface (so far taken to be a circular cylinder). Exhaustive numerical calculations have provided reliable comparisons of different field representations and have permitted a critical evaluation of their accuracy and sensitivity to error or to parameter changes. The results produced under this

contract are the most complete yet available, and they have yielded basic insights into the physical mechanisms that establish the concave surface field.

Two manuscripts, accepted for publication in IEEE Transactions on Antennas and Propagation, and attached in the Appendix, summarize these accomplishments which are therefore not detailed here:

1. "High Frequency Fields Excited by a Line Source Located on a Perfectly Conducting Concave Cylindrical Surface", by T. Ishihara, L.B. Felsen and A. Green, and

2. "High Frequency Fields Excited by a Line Source Located on a Concave Cylindrical Impedance Surface", by T. Ishihara and L.B. Felsen.

A third manuscript, almost completed, extends these studies to the three-dimensional case of point source excitation.

The following papers were given at technical meetings:

"Excitation of Large Concave Surfaces", by L.B. Felsen and A. Green, IEEE/AP-S International Symposium, University of Massachusetts, Amherst, Mass., October 10-15, 1976.

"Ground Wave Propagation in the Presence of Smooth Hills and Depressions", by L.B. Felsen and A. Green, AGARD Symposium on EM Propagation Characteristics of Surface Materials and Interface Aspects, held in Istanbul, Turkey, October 18-19, 1976 and published in the Symposium Proceedings.

"Effects of Smooth Elevations and Depressions on Ground Wave Propagation", by L.B. Felsen and T. Ishihara, URSI Symposium on Propagation in Non-Ionized Media, held in La Baule, France, April 28-May 6, 1977.

"High-Frequency Currents Excited by a Line Source Located on a Concave Cylindrical Surface", by L.B. Felsen and T. Ishihara, URSI International EM Wave Theory Symposium, Stanford University, Palo Alto, California, June 20-24, 1977.

"High-Frequency Fields Excited by a Line Source Located on a Concave Cylindrical Impedance Surface", by T. Ishihara and L. B. Felsen, 1978 International URSI/AP-S Symposium, Washington, D.C., May 15-19, 1978.

"High-Frequency Behavior of Concave Surfaces" by L. B. Felsen, Invited paper, 18 URSI General Assembly, Helsinki, Finland, August 1978.

APPENDIX

1. High Frequency Fields Excited by a Line Source Located on a
   Perfectly Conducting Concave Cylindrical Surface, T. Ishihara,
   L. B. Felsen and A. Green.

2. High Frequency Fields Excited by a Line Source Located on a
   Concave Cylindrical Impedance Surface, T. Ishihara and L. B. Felsen.

1. High Frequency Fields Excited by a Line Source Located on a Perfectly Conducting Concave Cylindrical Surface

by

T. Ishihara, L. B. Felsen and A. Green
Department of Electrical Engineering
Polytechnic Institute of New York
Farmingdale, New York 11735

Abstract

Alternative representations are obtained for the high frequency surface field excited on a perfectly conducting concave circular cylinder by an axial magnetic line current located on the surface. Included are ray optical, canonical integral, whispering gallery mode and near field formulations, and various combinations of these. Asymptotic evaluations in different parameter ranges lead to results with varying accuracy and physical content. Their utility is assessed by extensive numerical calculations and comparisons. Most intriguing is a form of the asymptotic solution that involves only a number of geometric optical rays and a number of whispering gallery modes.

I. Introduction

When high frequency fields impinge on a concave perfectly conducting surface, the induced surface currents can be well approximated by their physical optics values since the entire surface is illuminated. Phrased alternatively, the method of geometrical optics is adequate to describe the surface field behavior. However, when actual sources or induced equivalent sources (for example, at an edge termination) are located very near or on the surface, geometrical optics becomes inapplicable because the multiply reflected ray fields (Fig. 1) have caustics that lie near the boundary (Fig. 2). Therefore, it is necessary to account in some other manner for the fields that would be contributed by rays having undergone many reflections.

A systematic study of the problem can be undertaken on the prototype configuration of a circular cylinder. Since a thorough understanding of the axially independent two-dimensional case is essential for extension to three-dimensional fields, attention is focused here on the problem of excitation by a magnetic line current located on the concave surface and oriented parallel to the cylinder axis. Starting from a rigorous formulation of the Green's function problem, one may extract from the azimuthally periodic solution for the closed surface a portion[1] that describes only the propagation characteristics between points Q and P in Fig. 1. Results obtained therefrom are applicable to concave surface segments that are open, and they are in a form suitable for subsequent generalization to variable surface properties. This basic representation, given as a contour integral, is the starting point for the present study, which has as its goal the exploration of alternative field representations that are useful for calculation in various parameter ranges. Included are ray-optical, canonical

integral and whispering gallery mode (Fig. 3) solutions, and various combinations of these. Strong emphasis is placed on the physical interpretation of the results, and on their relative accuracy. Most pleasing from a physical standpoint is a field solution that comprises a mixture of (N+1) geometric optical rays and M whispering gallery modes, with criteria provided for the proper choice of N and M.

In the course of the presentation, reference is made to the sparse relevant literature on this problem[1-3]. For certain of the alternative representations, we have performed extensions and refinements of previous results but others obtained here, in particular, the above-mentioned ray and whispering gallery mode combination, are new. The conclusions derived from this study, supported by extensive numerical calculations, provide a thorough understanding, both physically and quantitatively, of the propagation characteristics of perfectly conducting concave cylindrical surfaces. Some extensions to non-circular and(or) surface impedance boundaries have been considered elsewhere[1,3,4], as has the case of point source excitation[5].

II. Alternative Field Presentations

A. Green's Function Formulation

We consider the prototype problem of line source radiation inside a perfectly conducting circular cylinder of radius $\underline{a}$. To make the analysis relevant to the propagation along concave surfaces in general, it is necessary to remove the azimuthal periodicity imposed on the fields in the cylindrical $\underline{\rho} = (\rho, \phi)$ geometry, where ρ represents the radial and ϕ the angular (azimuthal) coordinate. This can be done by extending the range of the ϕ coordinate from its physical periodic domain $0 \leq \phi \leq 2\pi$ into an infinite domain $-\infty < \phi < \infty$ [6]. Such an extension implies that angularly propagating waves originating at the source point (ρ', ϕ') are outgoing toward $|\phi| = \infty$; this "angular radiation condition" can be realized by placing at some angular location away from the source angle ϕ' a perfect absorber for angularly propagating waves. Such an absorber has, however, the undesired property of generating diffraction at the radial coordinate origin $\rho = 0$. Therefore, when considering propagation phenomena ascribable only to the cylinder surface, it is desirable to remove the spurious diffraction effects from the total field solution.

The line source Green's function in the cylindrical domain $0 < \rho < a$, $-\infty < \phi < \infty$, can be constructed by the method of separation of variables and expressed in its most general form as a contour integral involving the two one-dimensional characteristic Green's functions g_ρ and g_ϕ for the radial and angular domains, respectively [6]. When the Green's function is represented in terms of angularly propagating waves, the corresponding eigenmode spectrum in the radial domain involves a discrete (whispering gallery mode) and continuous portion [3]. The latter accounts in part for propagation phenomena associated with the portion of the concave boundary

lying between the source and observation points (this is the desired contribution), and in part for the spurious diffraction effects of the angular absorber. When the spurious effects are removed and cognizance is taken of the high-frequency nature of the analysis, one may show that the relevant propagation characteristics along the portion of the concave boundary lying between the source point Q and the observation point P in Fig. 1 are contained in the partial Green's function[1]

$$G(\underset{\sim}{\rho}, \underset{\sim}{\rho}') = \frac{1}{i(\pi ka)^2} \int_C \frac{e^{i\nu|\phi - \phi'|}}{H_\nu'^{(2)}(ka) J_\nu'(ka)} \, d\nu \qquad (1)$$

where k is the free-space wavenumber, the prime on the cylinder functions denotes the derivative with respect to the argument, and a time factor $\exp(-i\omega t)$ is implied. It has been assumed in (1) that P and Q both lie on the boundary (i.e., $\rho = \rho' = a$) and that the boundary condition requires that the normal derivative of the Green's function vanishes at $\rho = a$; this makes G proportional to the axial component of magnetic field. The contour C and the singularities of the integrand in the complex ν-plane are shown in Figure 4. Contributions from the pole singularities ν_m arising from

$$J_{\nu_m}'(ka) = 0, \qquad m = 1, 2, \dots \qquad (2)$$

are found to describe whispering gallery modes. While (2) has an infinite number of real solutions as indicated in Fig. 4, only those with $\mathrm{Re}\, \nu_m > 0$ represent spectral contributions in the angular transmission representation which includes also a continuous spectrum.

B. Whispering Gallery Mode and Continuous Spectrum Representation

The spectral representation comprising a discrete (whispering gallery mode) portion and a continuous portion may be obtained directly from (1) by deforming C in Fig. 4 into a contour extending along the imaginary ν axis:

$$G = \sum_{m=1}^{M_1} G_m + R_{M_1} \tag{3}$$

where M_1 is the total number of poles satisfying $\mathrm{Re}\,\nu_m > 0$ and

$$R_{M_1} = \frac{1}{i(\pi ka)^2} \int_{-i\infty}^{+i\infty} \frac{e^{i\nu|\phi-\phi'|}d\nu}{H_\nu^{\prime\,(2)}(ka)J_\nu^\prime(ka)} \approx \frac{1}{\pi} \int_0^\infty e^{-ka|\phi-\phi'|\sinh v}\,dv, \quad ka \gg 1 \tag{4a}$$

is the continuous spectrum. Following Wasylkiwskyj,[3] the first integral may be simplified to the second form shown and also to

$$\frac{1}{2}\left[\underline{H}_o(ks) - Y_o(ks)\right] \quad , \quad s = a|\phi-\phi'| \tag{4b}$$

where $\underline{H}_o$ is the Struve function and Y_o the Neumann function. Each residue contribution G_m represents a whispering gallery mode of the form

$$G_m = \frac{i}{ka} e^{i\nu_m|\phi-\phi'|} J_{\nu_m}(ka)\left[\frac{\partial}{\partial\nu} J_\nu^\prime(ka)\right]_{\nu_m}^{-1} \tag{5}$$

On use of the uniform asymptotic formulas given by

$$J_\nu(ka) \sim \sqrt{\frac{2}{ka\cos w}}\; \sigma^{\frac{1}{4}}\, \mathrm{Ai}[-\sigma] \quad , \quad \nu = ka\sin w$$

$$J_\nu^\prime(ka) \sim -\sqrt{\frac{2\cos w}{ka}}\; \sigma^{-\frac{1}{4}}\, \mathrm{Ai}^\prime[-\sigma]$$

$$\sigma^{3/2} = \frac{3}{2} ka \left[\cos w - (\frac{\pi}{2} - w)\sin w\right], \quad \mathrm{Re}\, w > 0 \tag{6}$$

which are justified here, one finds

$$G_m \sim \frac{\exp(iks \sin w_m + i\pi/2)}{ka(\pi/2 - w_m)\cos w_m} \ . \tag{7}$$

The roots w_m are determined by solution of the resonance equation

$$\cos w_m - (\pi/2 - w_m) \sin w_m = \frac{2}{3ka} \sigma_m^{3/2} \tag{7a}$$

where $Ai'(-\sigma_m) = 0$, $m = 1, 2, \ldots M_1$.

C. Ray-optical Representation

To generate a ray-optical formulation, one replaces $H_\nu^{'(2)}(ka)$ and $J_\nu'(ka) = \{H_\nu^{'(1)}(ka) + H_\nu^{'(2)}(ka)\}/2$ by their Debye asymptotic forms

$$H_\nu^{'(1,2)}(ka) \sim \sqrt{\frac{2\cos w}{\pi ka}} \ \exp\left\{ \pm ika[\cos w - (\tfrac{\pi}{2} - w)\sin w] \pm i\tfrac{\pi}{4} \right\} \tag{8}$$

$$\text{Re } w > 0, \ \left\{ ka[\cos w - (\tfrac{\pi}{2} - w)\sin w] \right\}^{2/3} >> 1 \tag{8a}$$

where $\nu = ka \sin w$. Utilizing the traveling wave expansion

$$\frac{1}{J_\nu'(ka)} = \frac{2}{H_\nu^{'(2)}(ka)} \sum_{n=0}^{\infty} (-1)^n r^n, \quad r = \frac{H_\nu^{'(1)}(ka)}{H_\nu^{'(2)}(ka)}, \quad |r| < 1 \ , \tag{9}$$

in conjunction with (8), one reduces (1) to a series of integrals

$$G = \sum_{n=0}^{\infty} {}' G_n \ , \tag{10}$$

where

$$G_n \sim \frac{1}{\pi} (-i)^n \int_{C_n'} \exp[ika \, q_n(w)] \ dw \tag{10a}$$

and

$$q_n(w) = |\phi - \phi'| \sin w + 2(n+1) \left[\cos w - (\frac{\pi}{2} - w) \sin w \right] . \qquad (10b)$$

The saddle points of $q_n(w)$, as obtained from $dq_n/dw = 0$, are

$$w_{sn} = \frac{\pi}{2} - \frac{|\phi - \phi'|}{2(n+1)} , \qquad \overline{w}_s = \frac{\pi}{2} , \qquad (11)$$

and thus lie on the real w axis between $w = 0$ and $w = \pi/2$. A typical path C'_n through the nth saddle point is shown in Figure 5. The original path mapped from the ν plane can be deformed into C'_n. The Debye approximations in (8) are valid in this relevant region of the complex w-plane. Use of the conventional saddle point formula for evaluation of the integral in (10a) yields

$$G_n \sim e^{i\pi/4} \sqrt{\frac{2}{\pi k}} (-i)^n \frac{e^{ikD_n}}{\sqrt{D_n}} \qquad (12)$$

where

$$D_n = 2(n+1) a \sin \left[|\phi - \phi'| / 2(n+1) \right] . \qquad (12a)$$

This result corresponds to a direct or multiply reflected ray as depicted in Figure 1. and could have been constructed directly by ray-optical techniques.

Although the series in (10), with (12), formally contains ray contributions with an arbitrarily large number of reflections, these are suspect since the saddle points, from which they are derived all cluster about $w = \pi/2$. Thus, the asymptotic method, whereby each saddle point is treated as isolated, is inadequate. Moreover, (8) becomes invalid as $w \to \pi/2$, thereby invalidating the simplification of the integrand, on which the saddle point evaluation is based. It is therefore necessary to truncate the number of legitimate ray-optical terms at some $n = N$ such that w_{sN} is sufficiently less than $\pi/2$.

D. Ray plus Canonical Integral Representation

In view of the above observations, one may employ instead of (9) the partial expansion

$$\frac{1}{J'_\nu(ka)} = \frac{2}{H'^{(2)}_\nu(ka)} \sum_{n=0}^{N} (-1)^n r^n + \frac{1}{J'_\nu(ka)} (-1)^{N+1} r^{N+1} \tag{13}$$

Substitution of (13) into (1) yields

$$G = \sum_{n=0}^{N} G_n + R_N \tag{14}$$

where

$$R_N = \frac{1}{i(\pi ka)^2} \int_C \frac{e^{i\nu|\phi-\phi'|}}{H'^{(2)}_\nu(ka)J'_\nu(ka)} r^{N+1} (-1)^{N+1} d\nu \tag{15}$$

The sum in (14) evidently describes ray contributions having experienced up to N reflections. The remainder integral R_N incorporates the cumulative effects of ray fields having been reflected more than N times. It should be noted that when the observation point approaches the source point so that $|\phi-\phi'| \to 0$, one has $\nu_s \to ka$ even for n = 0, and the ray representation fails altogether. When N = - 1, no ray contributions are extracted and (15) agrees with (1).

Several options are open for dealing with R_N. One possibility is to explore under what conditions the contributing range of the integrand is localized so that approximation methods may be used effectively. To this end, the cylinder functions are first replaced by their uniform asymptotic approximations in terms of Airy functions. From the behavior of the integrand over the contour C in the ν-plane or the contour C' in the w-plane, it may then be shown that the principal contribution to the integral arises from the vicinity of $\nu = ka$ or $w = \pi/2$ provided that the arc length parameter

$$\gamma = \left(\frac{ka}{2} \right)^{1/3} \frac{s}{a} \tag{16a}$$

and the number of rays are related by the criterion (note that we designate a ray having undergone N reflections as the $(N+1)$th ray)

$$\frac{\gamma}{2(2^{1/3}\Delta)^{1/2}} - 1 < (N+1) \leq \frac{\gamma}{2(2^{1/3}\Delta)^{1/2}} \tag{16b}$$

where $\Delta = \Delta(ka) = O(1)$ is chosen appropriately. When the left-hand side of the inequality is negative, i.e., in the region near the source, no ray-optical contributions are included. The first inequality in (16b) is required to assure that the integrand in (18a) decays away from $t = 0$. The second inequality in (16b) (and the inequality in (21a)) is required to validate use of the Debye approximations in the first term in (13), which yields the geometric optical ray contribution.

Our criterion in (16b), the utility of which is confirmed by the numerical calculations in Sec. III, differs somewhat from that obtained by Babich and Buldyrev[1]. The numerical factor Δ in the inequalities (16b), and also in (21a), is not rigidly fixed. This implies that the location of the point at which a geometric-optical ray field splits off from the remainder field can be varied. In each specific problem, the factor Δ should be chosen such that the discontinuity in the total field is a minimum when the new geometric-optical wave emerges. The estimated value of $\Delta = O(1)$ can be determined from a knowledge of the point of emergence of the direct ray. This point can be found by comparing the numerical results of the direct ray plus canonical integral representation here, or of the direct ray plus whispering gallery mode representation (Sec. E), with that of the exact solution (whispering gallery mode and continuous spectrum representation). In this manner, one finds from (16b) or (21a) with $N = 0$ that $\gamma \approx 3.1$ whence $\Delta \cong 2$ (see Figs. (8), (10) and (11)). This value of Δ is then used in (16b) to determine the splitting off points of the various reflected rays. It turns

out that the results are not very sensitive to the choice of Δ because of the overlap of the curves for various N. Therefore, Δ can be determined from the first overlap region for N = -1, N = 0, without the need of performing the comparison with the exact solution.

Changing variables to t via $\nu = ka + (ka/2)^{1/3} t$ and using

$$H'^{(1)}_{\nu}{}^{(2)}(ka) \sim - (\frac{2}{ka})^{2/3} w'_1(t), \quad J'_{\nu}(ka) \sim - (\frac{2}{ka})^{2/3} Ai'(t) \tag{17}$$

where $w_1(t) = Ai(t) \mp i Bi(t)$, one may write (15) as
$$\quad {}_2$$

$$R_N \sim \frac{(-1)^{N+1} e^{iks}}{2i\pi^2 ka} (\frac{ka}{2})^{2/3} I_N(\gamma) \tag{18}$$

where

$$I_N(\gamma) = \int_{C_t} \frac{e^{i\gamma t}}{Ai'(t) w'_2(t)} \left[\frac{w'_1(t)}{w'_2(t)} \right]^{N+1} dt \tag{18a}$$

The contour C_t in the t-plane is inferred from the mapping and Fig. 4 by observing that $\nu = ka$ corresponds to $t = 0$. The integral in (18a) is in a canonical form analogous to the Fock integral for convex surfaces. Tabulations exist for selected ranges of γ and N.[9] When N = -1, the resulting expression in (18) is a valid representation for G in the range of small γ. N = 0 defines the domain of the direct ray, N = 1 the domain of the direct plus singly reflected ray, etc.

E. Ray plus Whispering Gallery Mode Representation

An alternative possibility is to represent R_N as a whispering gallery mode sum plus an explicit remainder. If C is deformed into C_N in Fig. 4. M residues at the poles ν_m of the integrand lying between C and C_N

must be extracted. One finds

$$R_N = \sum_{m=1}^{M} G_m + R_{MN} \tag{19}$$

where G_m is given in (5) or (7). The remainder integral R_{MN} is the same as R_N except for the replacement of C by C_N. It may be shown (see Appendix) that the remainder integral R_{MN} can be approximated by

$$R_{MN} \approx -\frac{1}{2} G_N . \tag{20}$$

provided that observation poinsts are characterized by $w_{sN} \approx (w_M + w_{M+1})/2$, i.e., for saddle points w_{sN} well removed from the pole singularities (see Section III for a discussion on procedure when this condition is not satisfied). Thus,

$$G \sim \sum_{n=0}^{N} G_n + \sum_{m=1}^{M} G_m - \frac{1}{2} G_N \tag{21}$$

The number of rays, (N+1), is picked according to the criterion

$$N + 1 \leqq \frac{\gamma}{2(2^{1/3}\Delta)^{1/2}} \tag{21a}$$

F. Near Field and Infinite Plane Limits

Except for the whispering gallery mode plus continuous spectrum representation in Sec. B, which is not convenient for numerical computation, the other formulations cannot account for the limiting case $\gamma \to 0$ in (16a), which arises either when the observation point approaches the source point (s → 0 with a fixed) or when the radius of curvature becomes arbitrarily large (a → ∞ with s arbitrary but fixed). The latter limit traces the transition from a concave to a plane surface and, if a is allowed to become negative, from concave to convex. We have derived the transition functions

for these cases.

We begin with G expressed by (18), with $N = -1$, and use the Wronskian relation for the Airy functions together with Cauchy's theorem applied to the upper half of the t-plane to infer that, equivalently,

$$G \sim - \frac{e^{iks}}{2\pi ka} \left(\frac{ka}{2}\right)^{2/3} \int_{-\infty - i\delta}^{+\infty - i\delta} e^{i\gamma t} \frac{Ai(t)}{Ai'(t)} \, dt \tag{22}$$

Employing large argument expansions, one may show that

$$- \frac{Ai(t)}{Ai'(t)} \sim \sum_{j=0}^{10} \frac{a_j}{t^{(1+3j)/2}} + O(t^{-34/2}), \quad -\pi < \arg t < 0 \tag{23}$$

where $a_0, a_1, \dots a_{10}$ are given by

$$a_0 = 1, \ a_1 = -1/4 \ , \ a_2 = 7/32, \ a_3 = -21/64$$

$$a_4 = 0.7143531708 \ , \quad a_5 = -2.071282248 \ , \ a_6 = 7.557254769 \tag{23a}$$

$$a_7 = -33.32008068, \quad a_8 = 161.5948751 \ , \quad a_9 = -1019.868939$$

$$a_{10} = 6845.104932$$

Then by Laplace inversion of (22)[7]

$$G \sim \frac{i}{2} H_0^{(1)}(ks) \left\{ \sum_{j=0}^{10} b_j \gamma^{(3/2)j} + O(\gamma^{33/2}) \right\} \tag{24}$$

where $b_0, b_1, \dots b_{10}$ are given by

$$b_0 = 1 \quad , \quad b_1 = \sqrt{\pi} \ e^{-i\pi/4}/4 \ , \quad b_2 = -7i/60$$

$$b_3 = -7\sqrt{\pi} \ e^{i\pi/4}/512, \quad b_4 = -0.4398134 \times 10^{-2}$$

$$b_5 = -0.4109687 \times 10^{-3} \sqrt{\pi} \ e^{-i\pi/4} \ , \quad b_6 = 0.1122861 \times 10^{-3} i \ , \quad (24a)$$

$$b_7 = 0.9182121 \times 10^{-5} \sqrt{\pi} \ e^{i\pi/4} \ , \quad b_8 = 0.2093046 \times 10^{-5}$$

$$b_9 = 0.1637812 \times 10^{-6} \sqrt{\pi} \ e^{-i\pi/4} \ , \quad b_{10} = -0.3623427 \times 10^{-7} i$$

All the terms shown have been used for subsequent numerical evaluation of G.

Actually, the inversion yields for the factor outside the braces in (24) the large argument approximation of $(i/2)H_o^{(1)}(ks)$, the Green's function for an infinite perfectly conducting plane. By inserting the exact limiting value of $a \to \infty$, the formula in (24) may be applied as well in the near field of the source.

To trace the transition from concave to convex curvature when the distance s along the surface remains fixed, we allow $\underline{a}$ to change continuously from positive to negative values via the complex excursion $0 \leq \arg a \leq \pi$. To keep $s = a |\phi-\phi'|$ positive, it is necessary simultaneously to have $\arg |\phi-\phi'| = -\arg a$. Moreover, one must continuously deform the integration path in the complex t-plane to keep the integral convergent $(\exp(i\gamma t)$ oscillatory) when γ is allowed to become complex according to the rules stated above. These considerations lead to a straight line path along which $\arg t = -\pi/3, 2\pi/3$, when $\arg \underline{a} = \pi$. Changing variables $t = \mu \exp(i2\pi/3)$, one finds

$$G \sim \frac{e^{iks}}{2\pi ka} \left(\frac{ka}{2}\right)^{2/3} \int_{C_\mu} \frac{w_1(\mu)}{w_1'(\mu)} e^{i\gamma\mu} d\mu \tag{25}$$

where γ is again given by (16a) and the path C_μ proceeds along the real μ axis. The expression in (25) is the known result for the field on the surface of a convex perfectly conducting cylinder. By contour deformation about the singularities μ_p at $w_1'(\mu_p) = 0$, one derives the creeping wave series, and by expansion analogous to (23) and Laplace inversion the limiting transition as $\gamma \to 0$. Thus, one may track the field continuously as the curvature changes from concave to convex between fixed source and observation points on the surface.

III. Numerical Results

Extensive numerical computations have been performed for $ka = 10$, 30, 50, 100 and 1000 to check the accuracy and range of validity of the various formulations in Section II. Results are presented in Figs. 6 - 12 for $ka = 10$, 100 and 1000 only since all of the relevant formulas apply to $ka = 30$ and 50 with accuracy similar to that obtained for the larger values $ka = 100$, 1000.

Except for the low (ka) values $(ka = 10)$, the whispering gallery mode and continuous spectrum representation in (3), for arbitrary γ, has been taken as the reference solution, with which the other results are compared. The failure of this representation for low (ka), as evidenced by the oscillations in the curves in Fig. 8(a) for small γ, is attributed to difficulties in evaluating the eigenvalues of the whispering gallery modes with sufficiently high precision; for the larger (ka) values, the uniform approximations in (6) are adequate. A remarkable feature of this representation is the sensitivity of the field to the exact number M_1 of whispering gallery modes, as evidenced in Fig. 6 for $ka = 100$. Here, $M_1 = 32$, and any deviation from this number causes oscillations about the true field magnitude.

It can also be seen from Fig. 6 that as the number of whispering gallery modes approaches $M_1 = 32$, the field magnitude also approaches the true value. The continuous spectrum is necessary to establish the near field for moderate γ. Analytically, this means that the Neumann function in (4b) together with the discrete spectrum (whispering gallery modes) produces the proper singularity near the source point. Omission of the continuous spectrum leads to errors that can be assessed in Fig. 7.

The ray plus canonical integral representation in (14) is seen to provide an excellent approximation for all cases (i. e., for ka = 10, 100, 1000) as shown in Figs. 8(a)-(c) provided that the number of rays (N+1) is chosen according to the criterion in (16b). Because of the overlap of the curves for various N, no difficulty arises in switching from one formulation to the other as γ varies. Tabulations of the canonical integral in (18a) are given in reference 9 for the perfectly conducting boundary and for non-vanishing surface impedance. When ka is small, this representation may serve as a reference because it does not exhibit the sensitivity (see Fig. 8(a)) encountered with the whispering gallery mode and continuous spectrum formulation. As shown in Fig. 11(a), the ray plus canonical integral representation for small ka agrees well with the near field expansion in (24).

The most intriguing and physically most appealing formulation is based on the mix of (N+1) rays and M whispering gallery modes in (21). The whispering gallery modes plus the last term in (21) account for the field near the surface where geometrical optics becomes invalid. Because of the inequality (21a) that must be satisfied by the number of rays, N+1, the inclusion of multiply reflected rays requires larger separation γ between source and observation points. For any given N, as γ increases in its applicable range, a new whispering gallery mode must be included whenever the N-times reflected ray touches the caustic of that mode. The process for N=0 is depicted in Fig. 9a. The concentric circles show the modal caustics of the whispering gallery modes while the angle w_K represents the eigenvalue of the K-th mode. Within the ranges of P_1, P_2 and P_K, one must include the M=1, M=4 and M = K modes. Corresponding curves for $|G|$ are shown in Fig. 10. It should be noted that the direct ray plus whispering gallery mode representation yields a good approximation for $\gamma \geq 2(2^{\frac{1}{3}}\Delta)^{\frac{1}{2}}$. This

representation, however, is not recommended for large values of γ since many modes must then be included. For example, $N = 0$, $M = 24$, at $\gamma = 10$.

Inclusion of reflected rays, when appropriate, reduces the number of required whispering gallery modes, as depicted in Fig. 9(b). Thus, at the observation point $P(a,\phi)$, inclusion of only the direct ray $(N=0)$ requires six whispering gallery modes while inclusion of the direct and singly reflected rays $(N = 0,1)$ requires only a single mode, etc. Fig.9(b) also shows that the applicable range of the single mode plus ray representation becomes wider as the number of rays increases. As seen from Figs. 11(b)-(c), it is possible to represent the field accurately with only the lowest (most tightly bound) whispering gallery mode provided that a higher order reflected ray is included, when necessary, as γ increases. Accordingly, although (21) is a good representation for the ranges satisfying the inequality (21a), the simplest and physically most appealing expression will be (21) with the inequality (16b). Figs. 11(a)-(c) have been obtained with the inequality (16b). These results are surprisingly simple compared with the whispering gallery mode and continuous spectrum representation, for which 32 modes for $ka = 100$ and 319 modes for $ka = 1000$ must be included in order to obtain accurate field values. In Figs. 11(a)-(c), the number indicated along the curves should be read as follows: for example, $M=2$ $[N=1]$ denotes the range wherein the direct and singly reflected rays plus 2 whispering gallery modes are applicable, while the circles indicate the starting points of the relevant intervals.

Analytically, the emergence of a whispering gallery mode (contact of ray and modal caustic) is characterized by the coalescence of a pole and a saddle point in the remainder integral R_{MN}. Therefore, the field in (21)

is discontinuous at these points. The discontinuity can be avoided on use of a Fresnel integral transition function[8] in the vicinity of these γ values. However, we have found that continuity can be established by using the simple result when pole and saddle point coincide (this corresponds essentially to the midpoint between the two discontinuous endpoints) and then resorting to a perturbation expansion.

The ray and whispering gallery mode representation is invalid in the near field but it can there be joined to the near field expansion in (24). Concerning the latter, it should be noted in Fig. 12 that inclusion of more perturbation terms does not lead to continuing improvement or extension of the range of validity; for $ka = 100$, the perturbation terms up to $\gamma^{21/2}$ seem to give the best result. The near field forms with 8 perturbation terms are shown in Figs. 11(a)-(c) for $ka = 10$, 100 and 1000, respectively. From each figure, one can see that the changeover from the near field form to the direct ray plus lowest whispering gallery mode (i.e., $M=1$) representation can be performed at the crossover with negligible error.

IV. Conclusions

This analytical study of the characteristics of the surface field induced on the concave side of a perfectly conducting circular cylinder by a magnetic line source located on the surface has furnished a basic understanding of the propagation mechanisms that are operative in various parameter ranges involving source and observation point location, cylinder radius and wave frequency. Alternative representations of the field solution have been given and their relative accuracies assessed by extensive numerical calculation. The results have been discussed in detail in Section III. They permit, in particular, a quantitative appraisal of when, and under what circumstances, geometrical optics begins to play a role, and how the geometric optical field must be modified to account either for near field effects or for improperly formulated ray fields that have undergone many reflections. Quite remarkably, the latter can be accounted for by inclusion of only a single (the most tightly bound) whispering gallery mode and a partial ray field, although other possibilities exist that incorporate several whispering gallery modes. The asymptotic field solutions have been cast in a form that permits generalization to variable surface curvature or variable surface impedance[4], although some questions remain to be resolved.

Calculations for surfaces with finite surface impedence Z have also been performed, as have tabulations of the numerically evaluated canonical integral, for $Z = 0$ and selected values $Z \neq 0$. These results will be presented elsewhere[9].

Appendix - The Remainder Integral R_{MN}.

As noted in the text, the remainder integral R_{MN} is the same as R_N in (15) except for the replacement of C by C_N in Fig. 4. With the aid of the Wronskian relation

$$\frac{1}{i\pi \, ka \, J_\nu'(ka) \, H_\nu'^{(2)}(ka)} = \frac{1}{2}\left(\frac{J_\nu(ka)}{J_\nu'(ka)} - \frac{H_\nu^{(2)}(ka)}{H_\nu'^{(2)}(ka)}\right) \quad , \tag{26}$$

R_{MN} can be represented by

$$R_{MN} = \frac{(-1)^{N+1}}{2\pi ka} \int_{C_N}\left(\frac{J_\nu(ka)}{J_\nu'(ka)} - \frac{H_\nu^{(2)}(ka)}{H_\nu'^{(2)}(ka)}\right) r^{N+1} e^{i\nu \, |\phi-\phi'|} \, d\nu \tag{27}$$

Along the contour C_N, one may use in the integrand the Debye asymptotic formulas (see (8), and similarly for the undifferentiated cylinder functions) to obtain

$$R_{MN} \sim \frac{(-i)^{N+1}}{2\pi} \int_{C_N'}\left(\tan\left\{ka[\cos w - (\tfrac{\pi}{2}-w)\sin w] + \tfrac{\pi}{4}\right\} - i\right) e^{ikaq_N(w)} \, dw \tag{28}$$

where $q_N(w)$ and w_{sN} are given in (10b) and (11), respectively. If $w_{sN} \approx (w_{M+1} + w_M)/2$, the asymptotic evaluation involving the tangent function in the integrand of (28) yields a negligible contribution compared with the remaining term. In this case, referring to (10a) and (12),

$$R_{MN} \approx -\frac{1}{2} G_N \tag{29}$$

REFERENCES

1. BABICH, V. M. and BULDYREV, V. S. 1972. Asymptotic Methods of Short Wave Diffraction. Moscow, USSR: Nauka, Chapter 11, Section 4.

2. BULDYREV, V. M. and LANIN, A. I., Jan. 1975. "Asymptotic Formulas for a Wave Propagating Along a Concave Surface; Limits of Their Applicability." Radio Tekh. Elektron. Vol. 20.

3. WASYLKIWSKYJ, W., July 1975. "Exact and Quasi-Optic Diffraction within a Concave Cylinder," IEEE Transactions on Antennas and Propagation, Vol. AP-23, No. 4, pp. 480-492.

4. FELSEN, L. B. and GREEN, A., "Ground Wave Propagation in the Presence of Smooth Hills and Depressions," paper presented at the AGARD Symposium on EM Propagation Characteristics of Surface Materials and Interface Aspects, held in Istanbul, Turkey, October 18-19, 1976. Published in the Symposium Proceedings.

5. FELSEN, L. B. and ISHIHARA, T., "Effects of Smooth Elevations and Depressions on Ground Wave Propagation," paper presented at URSI Comm F Open Symposium on Propagation in Non-Ionized Media, held in La Baule, France, April 28-May 6, 1977.

6. FELSEN, L. B. and MARCUVITZ, N., 1973, Radiation and Scattering of Waves. Englewood Cliffs, NJ: Prentice Hall, Inc., Sections 2.3, 3.4.

7. HASSERJIAN, G and ISHIMARU, A., May-June 1962. "Currents Induced on the Surface of a Conducting Circular Cylinder by a Slot," J. Res. Nat. Bur. Stand., Vol. 66D No. 3, pp. 335-365.

8. FELSEN, L. B. and MARCUVITZ, N., Ibid., Chapter 4

9. ISHIHARA, T., GREEN, A. and FELSEN, L. B., "Surface Fields on a Concave Impedance Boundary," in preparation.

FIGURE CAPTIONS

FIG. 1   Direct and multiply reflected rays for a circular boundary.

FIG. 2   Reflected ray caustics.

FIG. 2(a)   Caustics A_n for rays reflected n times; these ray contributions are confined to the region between A_n and the boundary.

FIG. 2(b)   Caustic formation due to singly and doubly reflected rays.

FIG. 3   Whispering gallery mode: modal field, modal rays and caustic

FIG. 4   Integration path and singularities in complex ν-plane. **x** -- zeros ν_p of $H_\nu'^{(2)}(ka)$; $\cdots$-- zeros ν_m of $J_\nu'(ka)$. C_n is the steepest descent path through ν_{sn}.

FIG. 5   Integration paths and singularities in complex w-plane ($\nu = ka \sin w$). C' corresponds to C in Fig. 4 and can be deformed into the steepest descent path C_n' through w_{sn}. $\cdots$-- zeros w_m of $J_\nu'(ka)$; the poles w_p are not shown.

FIG. 6   Whispering gallery (W.G.) modes plus continuous spectrum.

FIG. 6(a)   Few modes.

FIG. 6(b)   Many modes.

FIG. 7   Effect of continuous spectrum

FIG. 8   Ray plus canonical integral representation. Both the γ and $|\phi-\phi'|$ coordinates are indicated. The ranges in γ and $|\phi-\phi'|$ corresponding to N = -1 (no geometric-optical ray) in (14), N = 0(1 ray), N = 1(2 rays) and N = 2(3 rays) are as shown.

———— whispering gallery modes and continuous spectrum

•—•—• $|G| = |R_{N=-1}|$. — · —— · —— · — $|G_{N=0}+ R_{N=0}|$

— ·· —— · — $|\sum_{n=0}^{1}G_n+ R_1|$ — · —— ·· —— · — $|\sum_{n=0}^{2}G_n + R_2|$

FIG. 8(a)   ka = 10

FIG. 8(b)   ka = 100

FIG. 8(c)   ka = 1000

FIG. 9   Geometrical interpretation of direct ray plus whispering gallery mode representation

FIG. 9(a)   N = 0 (direct ray only)

FIG. 9(b) $N = 0, 1, 2$

FIG. 10   Direct ray plus whispering gallery mode representation.
$M = K$ indicates point of emergence of K-th W.G. mode.
The solid curve is calculated from (3).

FIG. 11   Ray plus whispering gallery mode representation. The solid
curves serve as reference solutions. Here, the $|\phi - \phi'|$
coordinate is not shown since it has been depicted in Figure 8.

$M=K[N=0]$
o—·—·—·— $|G| = \left| \frac{1}{2} G_{N=0} + \sum_{m=1}^{K} G_m \right|$

$M=K[N=1]$
o—•—···—··· $|G| = \left| \sum_{n=0}^{1} G_n + \sum_{m=1}^{K} G_m - \frac{1}{2} G_{N=1} \right|$

$M=1[N=2]$
o—··—···— $|G| = \left| \sum_{n=0}^{2} G_n + G_m - \frac{1}{2} G_{N=2} \right|$

- - - - - - - - -   near field form

FIG. 11(a) $ka = 10$ ($M_1 = 3$). The solid curve is calculated from (14) and
(18).

FIG. 11(b) $ka = 100$ ($M_1 = 32$). The solid curve is calculated from (3).

FIG. 11(c) $ka = 1000$ ($M_1 = 319$). The solid curve is calculated from (3).

FIG. 12   Near field form. $ka = 100$
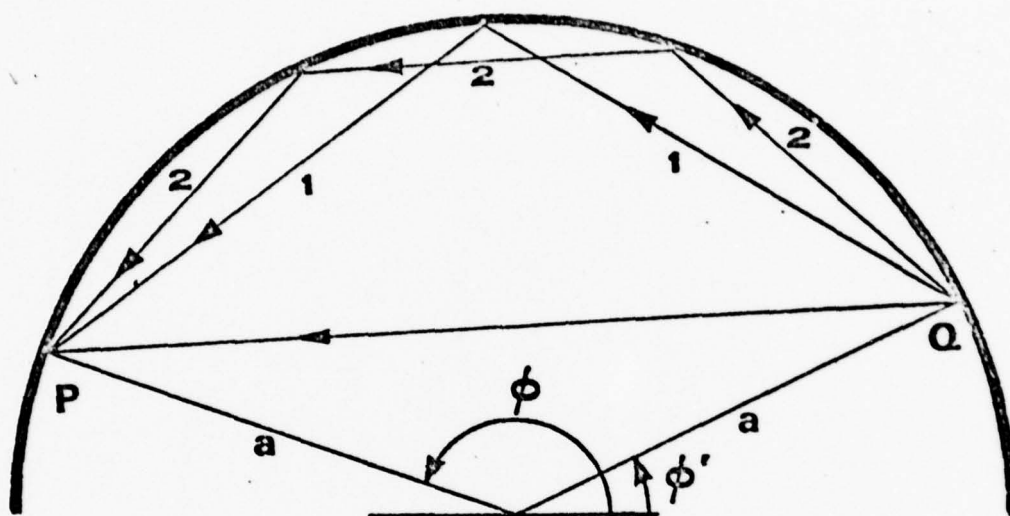
FIG. 1
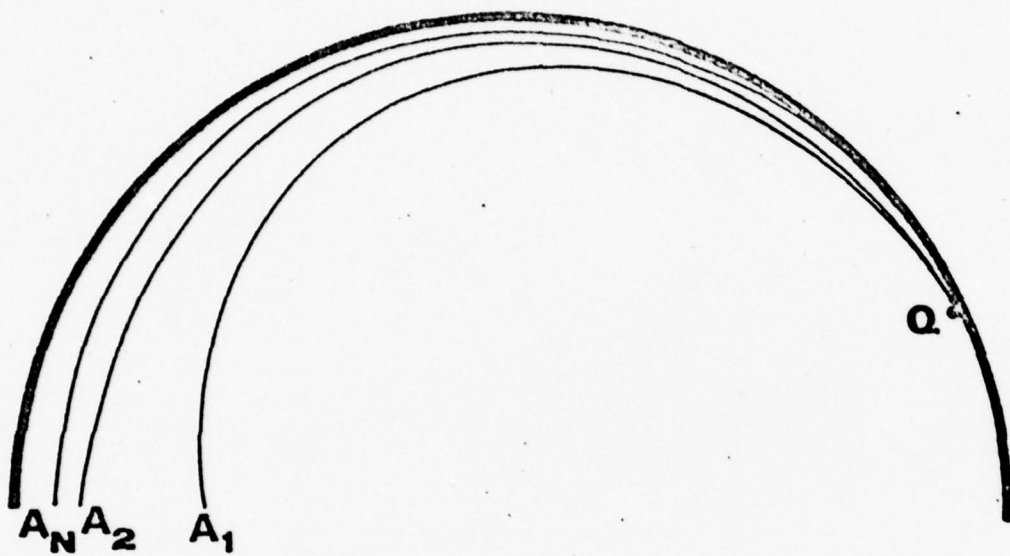
FIG. 2 (a)
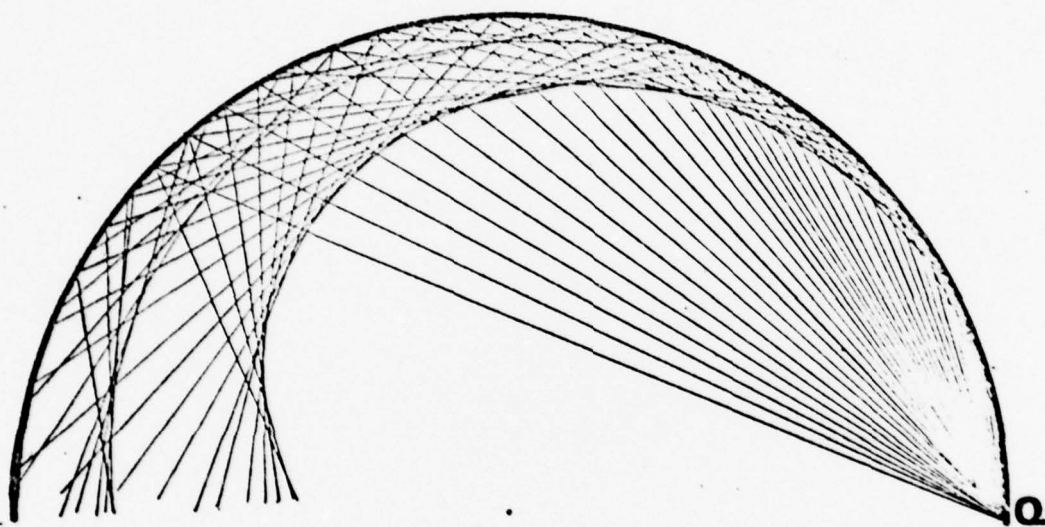
FIG.2 (b)

FIG. 3

FIG. 4

FIG. 5

FIG. 6 (a)

ka = 100

30 ·—··—··— ⎫
31 ·—·—·— ⎬ W. G. modes and
32 ——— ⎭ continuous spectrum

FIG. 6(b)
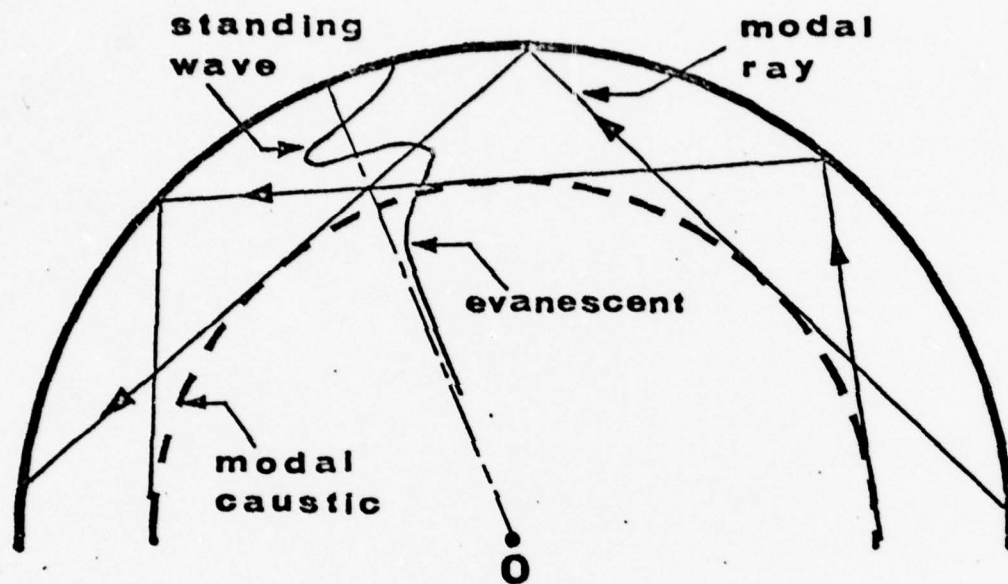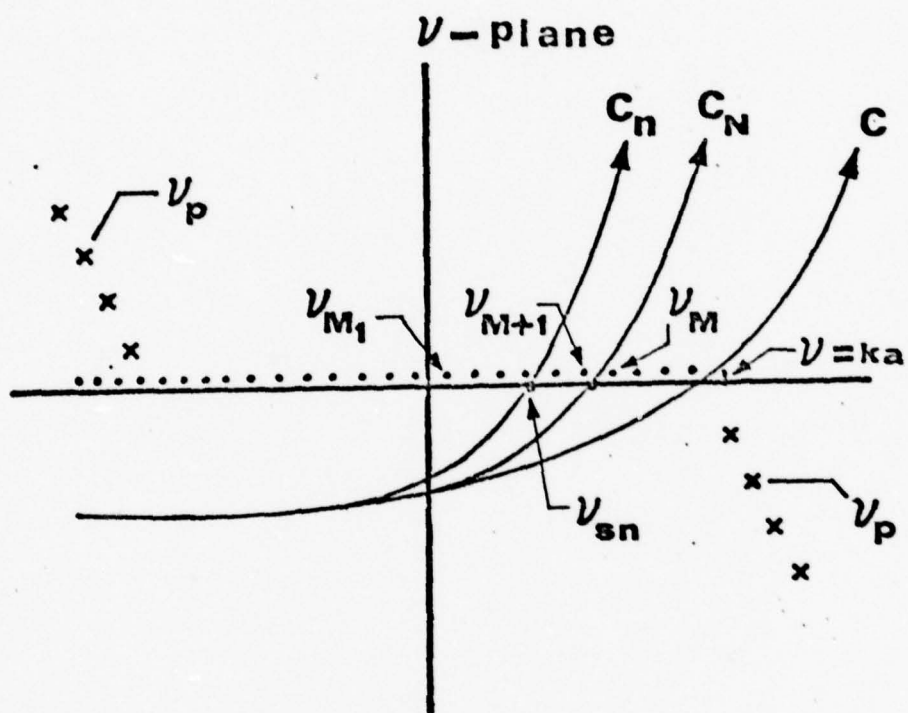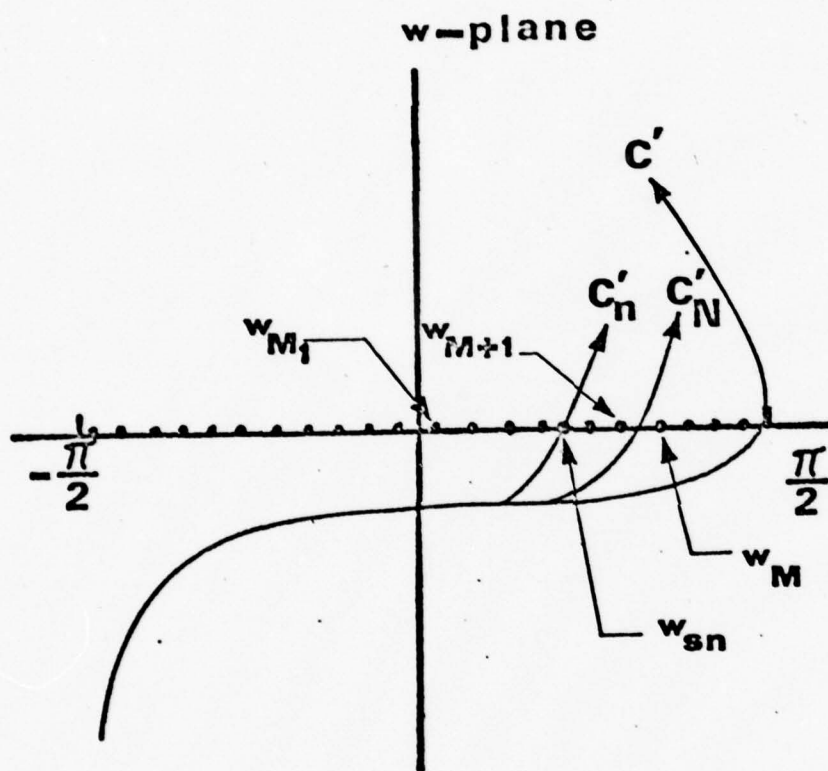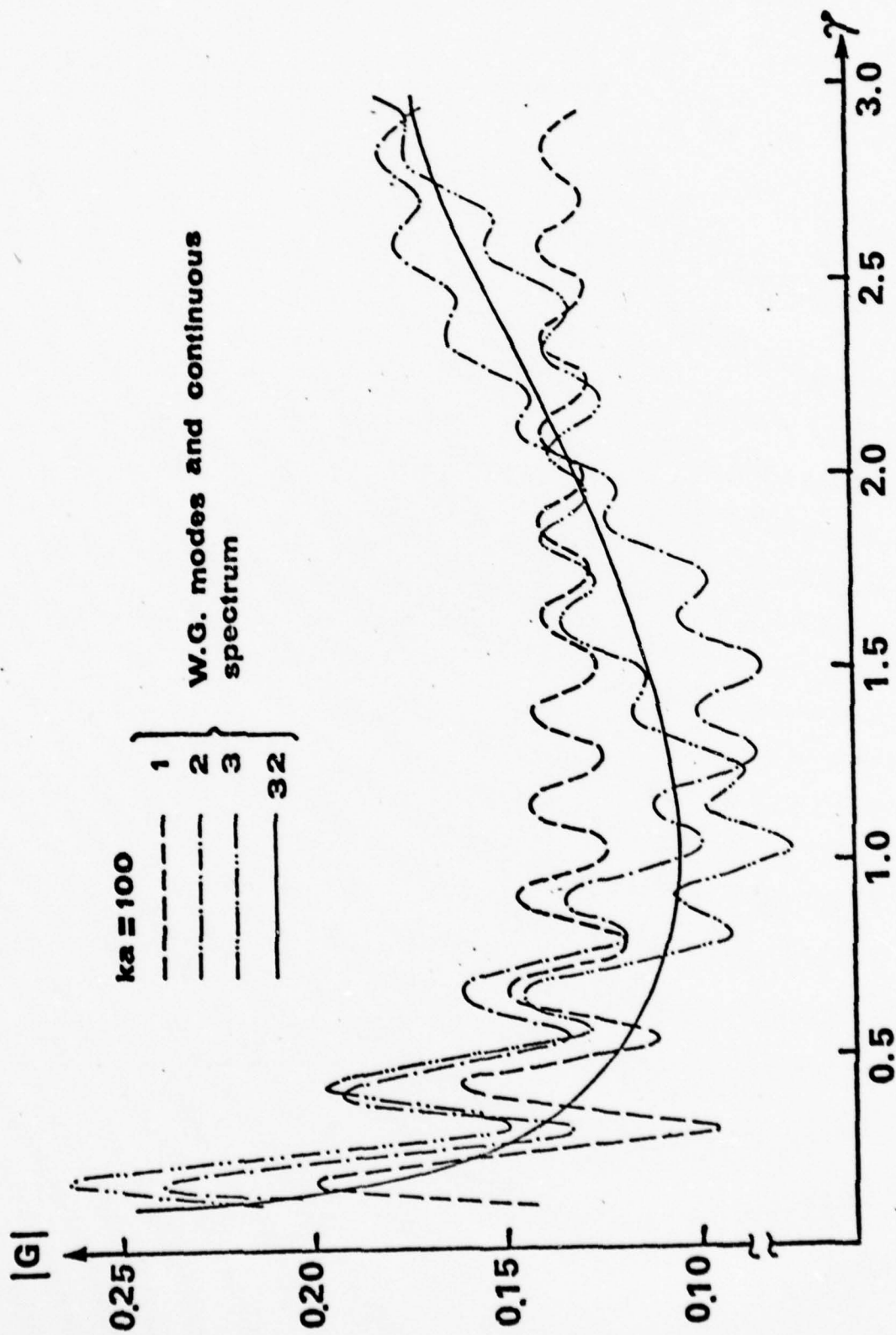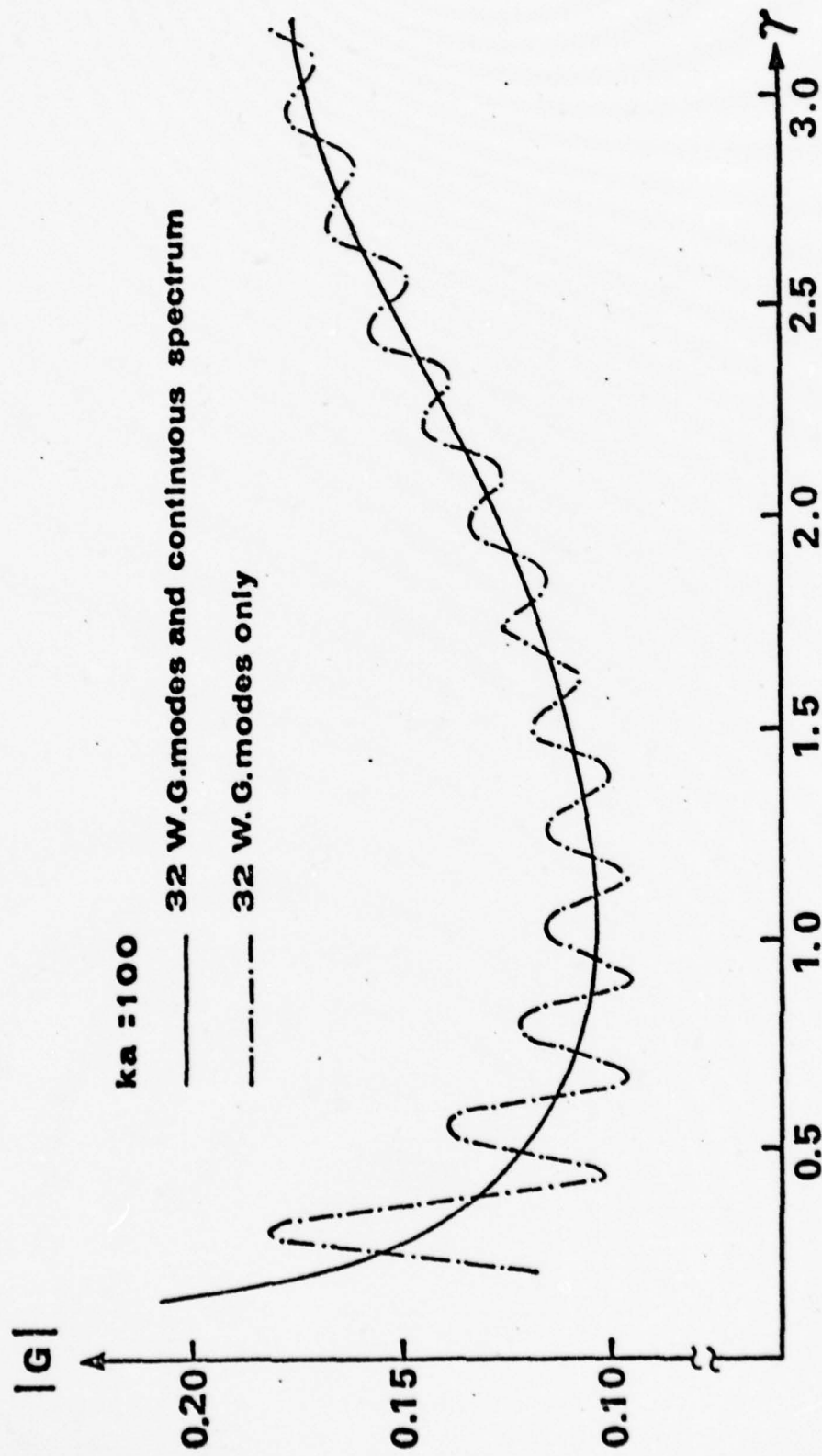
FIG. 7
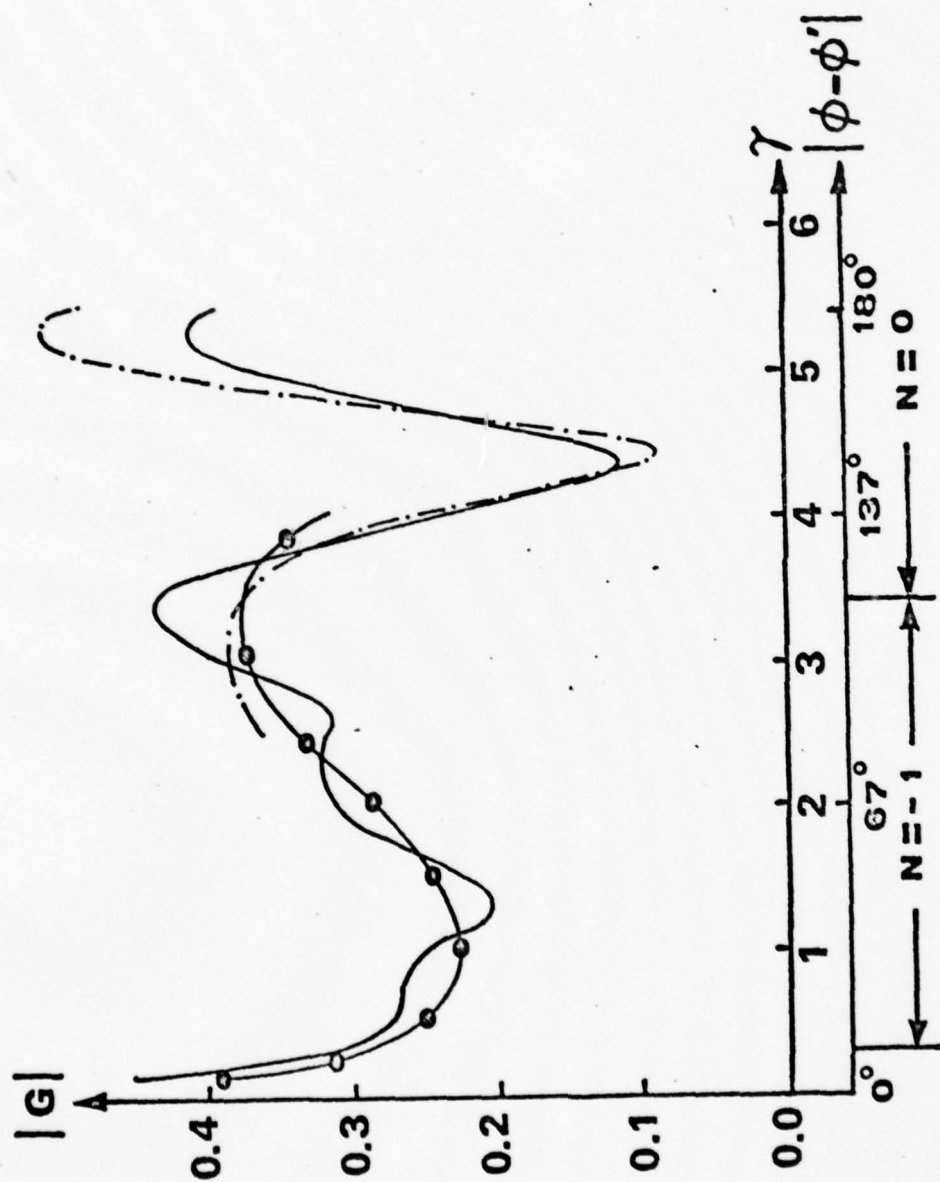
FIG.8 (a)
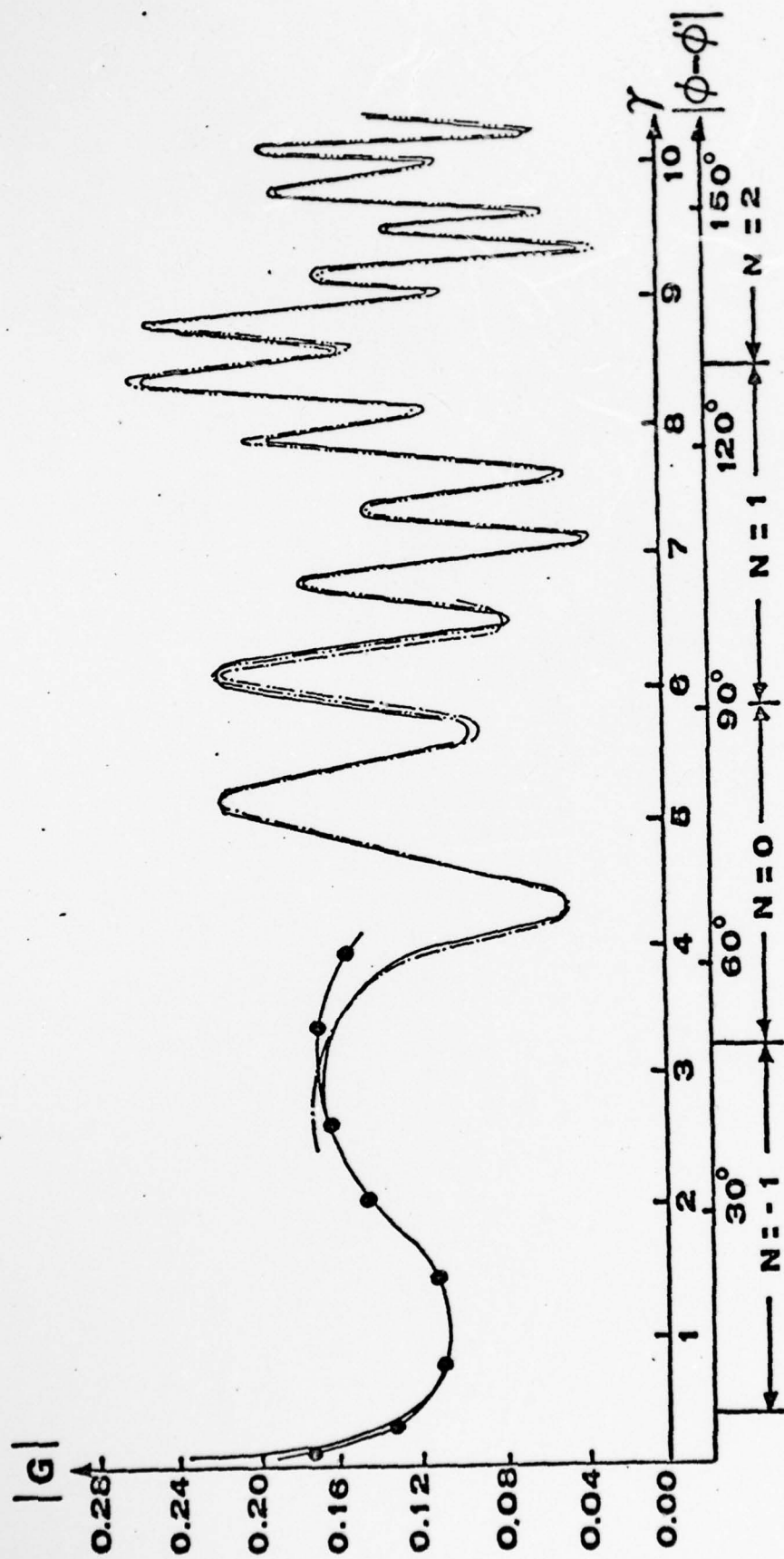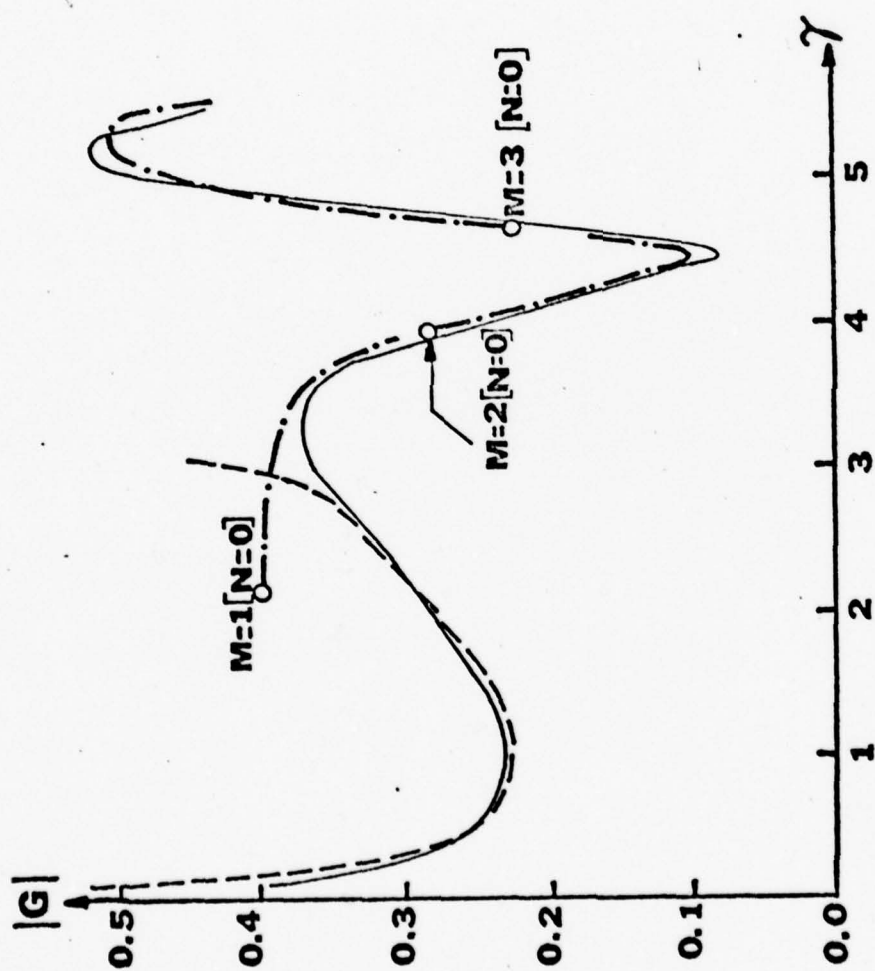
FIG. 8 (b)
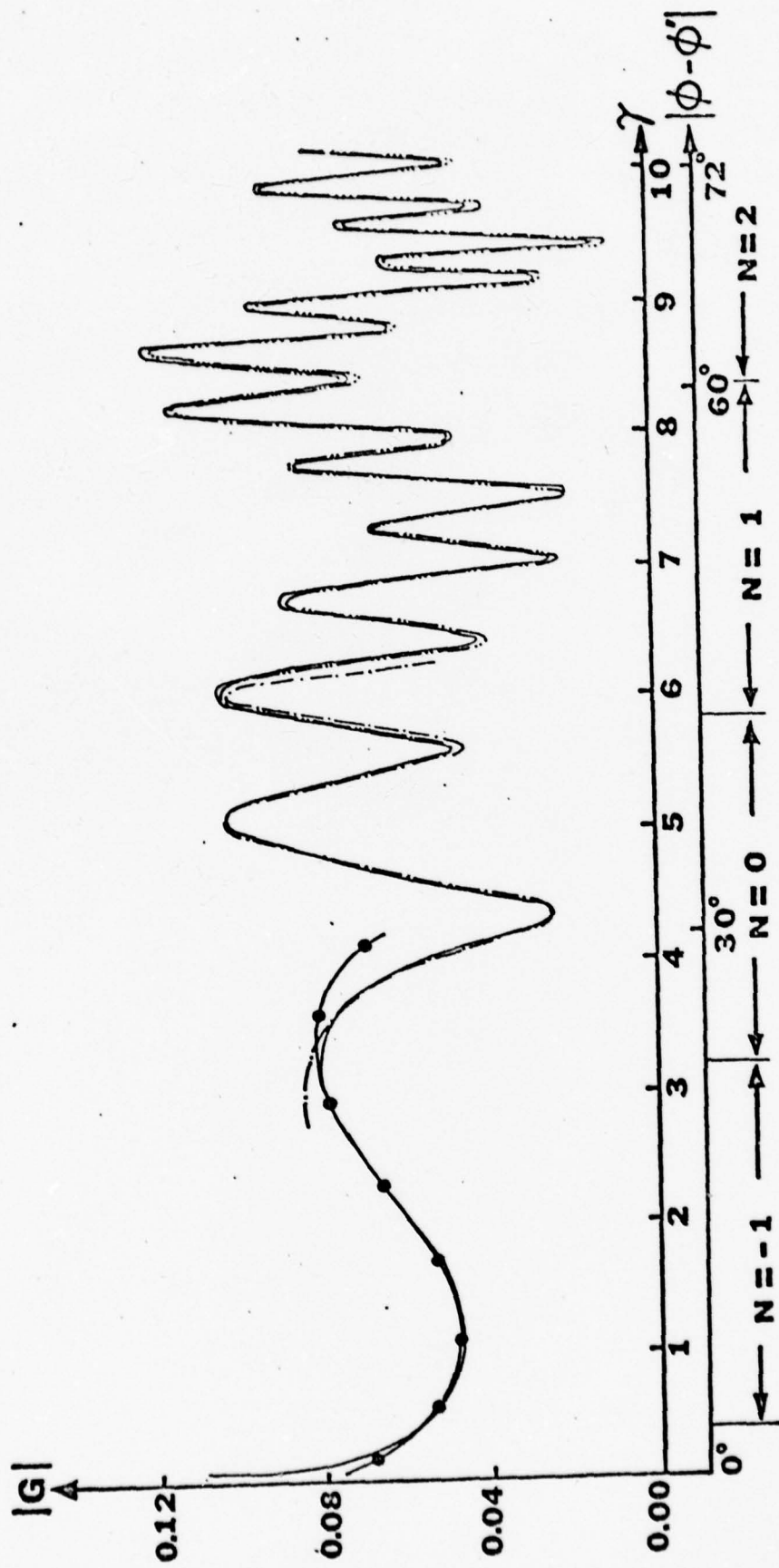
FIG.8(c)
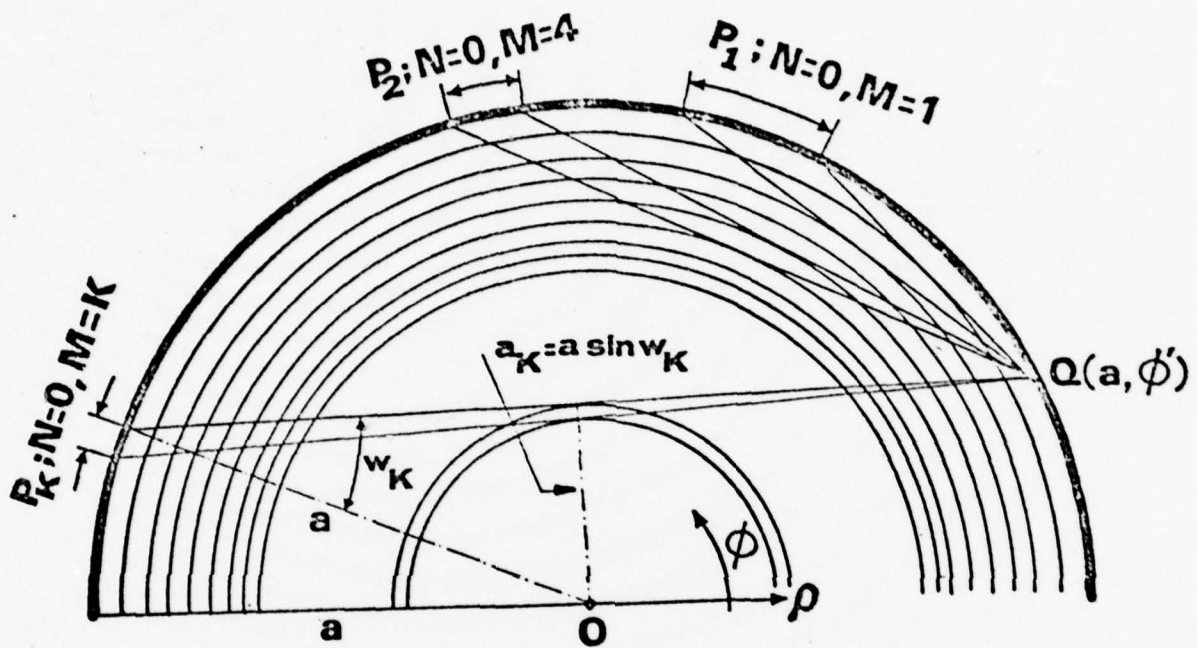
FIG. 9(a)
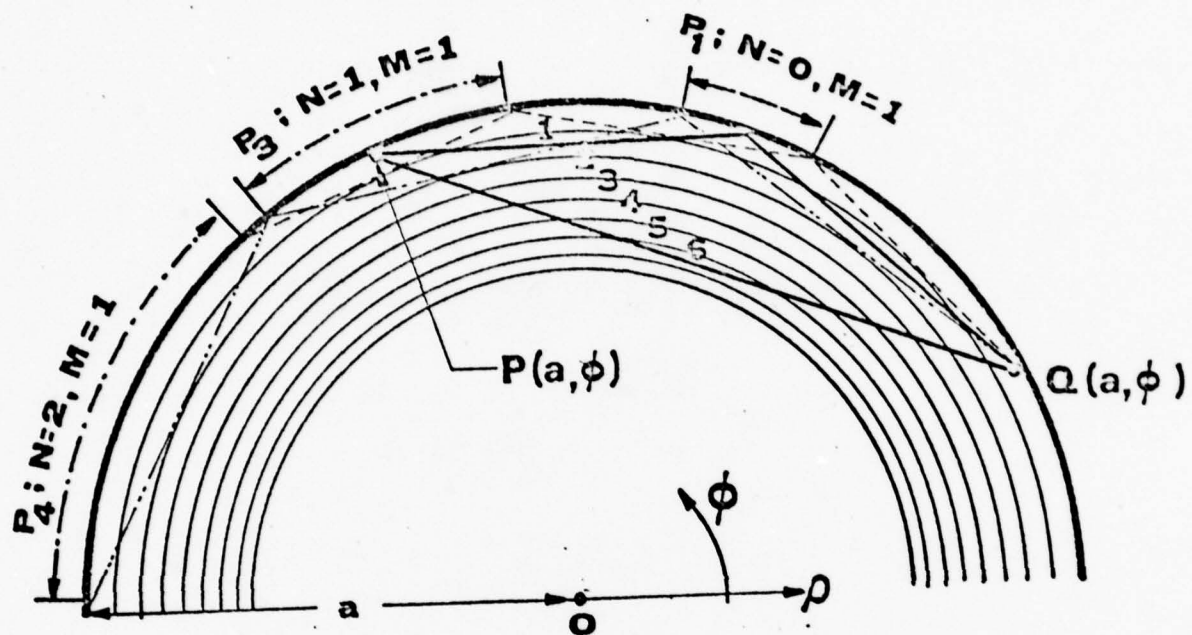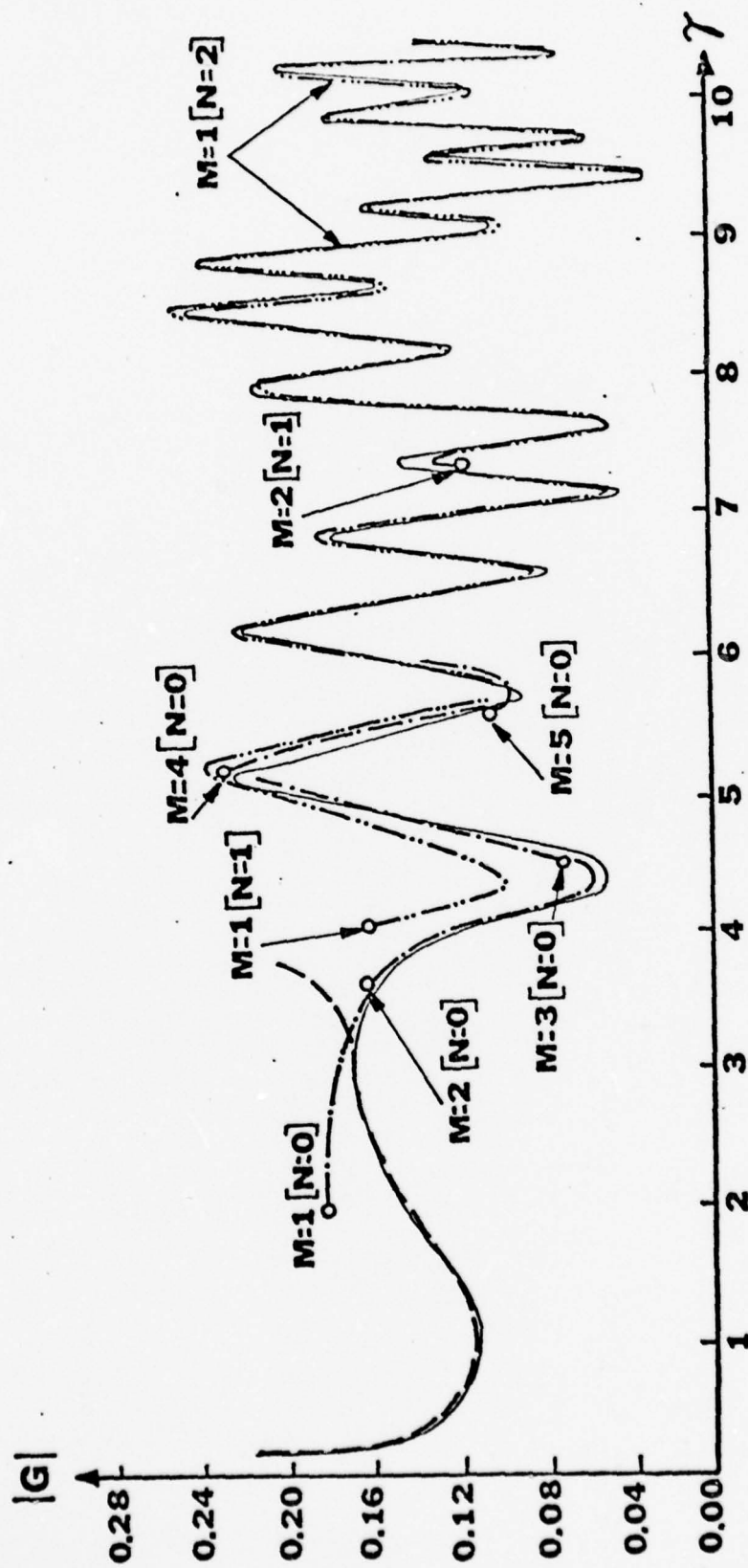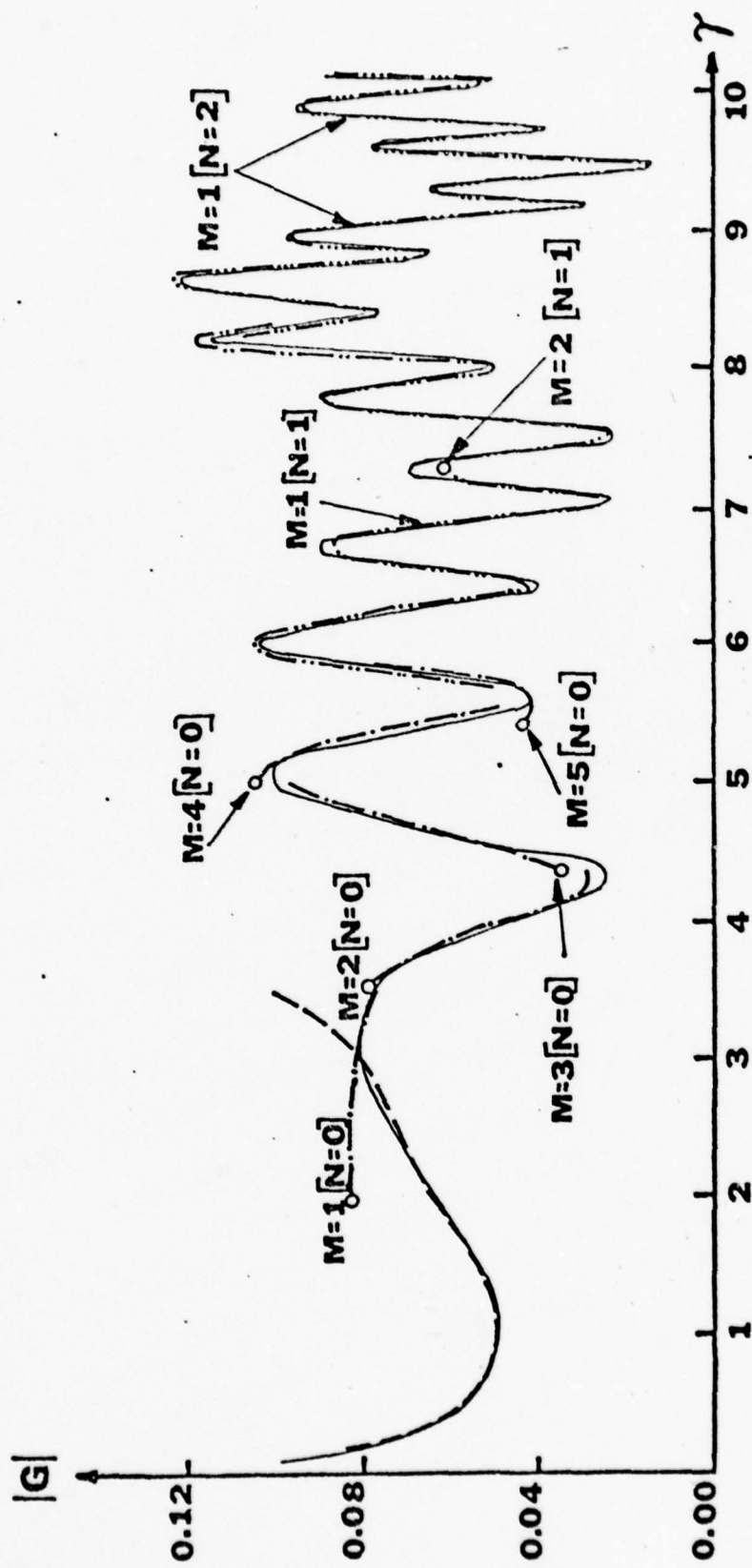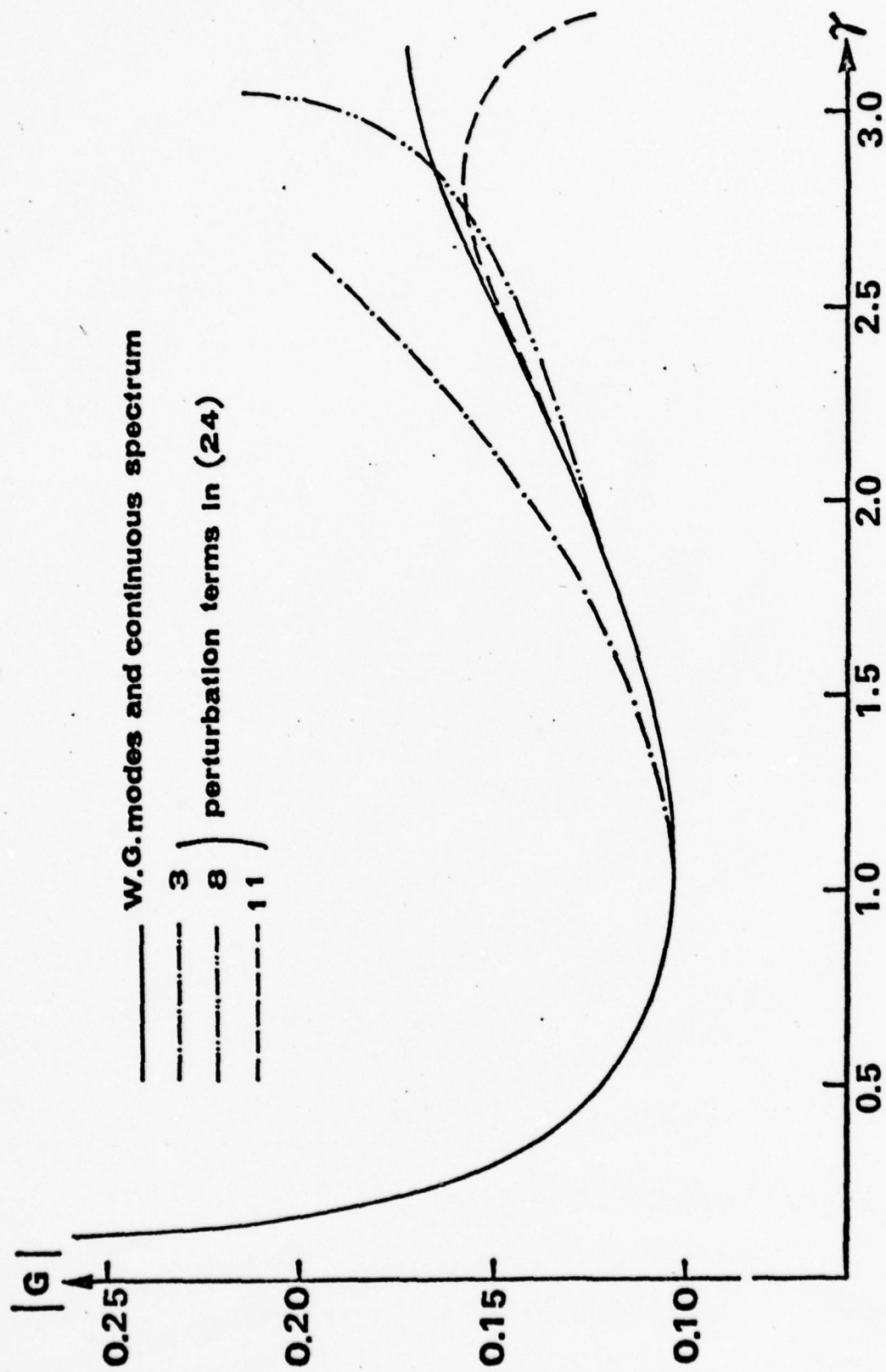
FIG. 9(b)
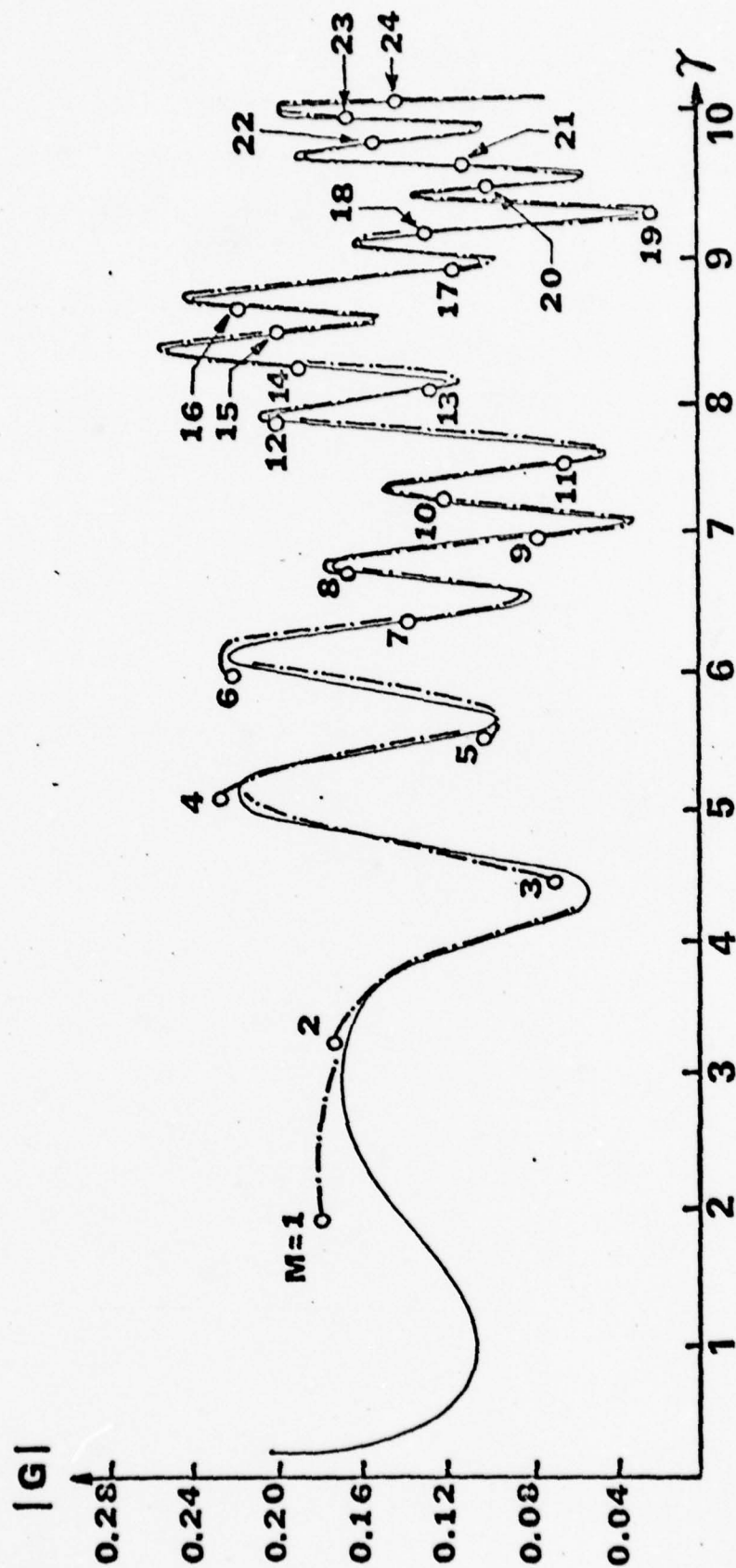
FIG.10

FIG.11(a)

FIG.11(b)

FIG.11(c)

FIG.12

2. High Frequency Fields Excited by a Line Source
Located on a Concave Cylindrical Impedance Surface

by

T. Ishihara and L. B. Felsen
Department of Electrical Engineering
Polytechnic Institute of New York
Brooklyn, New York 11201

Abstract

A previous study of high frequency currents induced by a line source
on a perfectly conducting concave cylindrical surface is extended to the case
of non-vanishing surface impedance Z_s. Alternative field representations
are formulated and evaluated asymptotically as combinations of ray optical,
whispering gallery mode, surface wave, continuous spectrum, and canonical
integral contributions. Numerical calculations provide an insight into the
accuracy and utility of the various formulations. Sufficiently far from the
source point, a combination of ray optical fields and tightly bound whisper-
ing gallery modes was previously found to be a most appealing form when
$Z_s = 0$. As the surface impedance becomes more dissipative, the whisper-
ing gallery modes are weakened by attenuation and eventually render the
ray optical fields adequate by themselves. A representation in terms of
rays and a canonical integral is found to be useful for all parameter ranges.
The canonical integral has been evaluated numerically and tabulated.

I. Introduction

When high-frequency fields impinge on a concave surface with large radius of curvature, the induced fields thereon differ markedly from those for the well explored convex case. A recent study[1] has dealt in detail with the two-dimensional problem posed by line source excitation on the interior boundary of a perfectly conducting circular cylinder. Alternative field representations, accounting only for propagation phenomena on the surface segment between source and observation points, were formulated and evaluated asymptotically. The field expressions so obtained were interpretable physically in terms of constituents involving whispering gallery modes, ray-optical fields, near field effects, continuous spectrum and canonical integral contributions. Extensive numerical comparisons showed the accuracy and range of applicability of each. This investigation has provided fundamental physical and quantitative insight into the field behavior on the perfectly conducting boundary.

In the present paper, the analysis is extended to accommodate surfaces with non-vanishing surface impedance Z_s. Because the alternative field representations (Section II) for $Z_s \neq 0$ are derived by the same techniques as those for $Z_s = 0$, the presentation is kept concise, with frequent reference made to the earlier study[1] for some of the details. Representative numerical calculations in Section III show how increasing surface impedance affects the surface field. When losses are appreciable, the closely bound whispering gallery modes are rapidly attenuated, leaving a properly formulated ray-optical field as the dominant and adequate contributor.

II. Alternative Representations

A. Basic Green's Function

The relevant magnetic line source Green's function for the interior of a circular cylinder with radius $\underline{a}$ and constant surface impedance Z_s is formulated in an infinite angular space wherein the azimuthal coordinate ϕ ranges from $-\infty$ to $+\infty$.[2] With the source point located at (ρ', ϕ') in a cylindrical (ρ, ϕ) coordinate system, the Green's function satisfies the inhomogeneous wave equation

$$\left(\frac{1}{\rho} \frac{\partial}{\partial \rho} \rho \frac{\partial}{\partial \rho} + \frac{1}{\rho^2} \frac{\partial^2}{\partial \phi^2} + k^2\right) G(\underset{\sim}{\rho}, \underset{\sim}{\rho'}) = -\frac{1}{\rho} \delta(\phi - \phi') \delta(\rho - \rho') \qquad (1)$$

with an "angular radiation condition" in the ϕ direction, and the radial boundary condition

$$\frac{\partial}{\partial \rho} G = ikZ'G \text{ at } \rho = a \; ; \qquad\qquad G \text{ finite at } \rho = 0 \qquad (1a)$$

Here $Z' = Z_s/Z_o$ is a normalized surface impedence, and Z_o is the impedance of free space. A time factor $\exp(-i\omega t)$ is suppressed.

Expressing the Green's function G as a contour integral and removing diffraction effects at the origin arising from the "angularly matched" condition[2], one obtains a modified form that contains only the essential propagation phenomena from the source point to the observation point in the presence of a cylindrical boundary segment. When the source and observation points are both located on the impedance boundary (i.e., $\rho = \rho' = a$), the modified Green's function G becomes

$$G = \frac{1}{i(\pi ka)^2} \int_C \frac{\exp(i\nu |\phi - \phi'|)}{[J_\nu'(ka) - iZ'J_\nu(ka)][H_\nu^{(2)'}(ka) - iZ'H_\nu^{(2)}(ka)]} \, d\nu \qquad (2)$$

where k is the free-space wavenumber, and the prime on the cylinder functions denotes the derivative with respect to the argument. The contour C and the singularities of the integrand in the complex ν-plane are shown in Fig. 1. In the lossless limit $Z' = 0$, this formulation reduces to the one in reference 1.

Anticipating subsequent contour deformation in the complex ν-plane, we examine the location of the pole singularities ν_m determined by the resonance equation

$$J'_{\nu_m} (ka) - iZ' J_{\nu_m} (ka) = 0, \quad m = 1, 2, \ldots, M_1, \quad \mathrm{Re}\,\nu_m > 0 \tag{3}$$

These poles in the integrand of (2) describe whispering gallery modes. For the special cases $\arg Z' = \pm 90^{\circ}$, the roots ν_m are real. If for $\arg Z' = -90^{\circ}$, the magnitude $|Z'|$ of the normalized impedance is greater than a certain value, one finds for the first root $m=1$ that $\nu_1 > ka$. The corresponding field contribution then describes a surface wave that can exist also on a plane boundary. It is interesting to note that all of the whispering gallery modes represent fast waves when the boundary is perfectly conducting.[1] However, for $Z' \neq 0$, there may exist slow-wave type whispering gallery modes with $\mathrm{Re}\,\nu_m > ka$, which become surface waves when $\mathrm{Im}\,\nu_m = 0$, in addition.

To facilitate the numerical evaluation of the poles in (3), it is convenient to separate the domain $\mathrm{Re}\,\nu_m > 0$ into two parts. In one of these, where $|\nu| \approx ka$, the Fock approximations for the bessel functions are applicable:

$$J_\nu (ka) \sim (2/ka)^{\frac{1}{3}} Ai(t) \,, \qquad J'_\nu (ka) \sim -(2/ka)^{\frac{2}{3}} Ai'(t)$$

$$H^{(1,2)}_\nu (ka) \sim (2/ka)^{\frac{1}{3}} w_{1,2}(t) \,, \qquad H'^{(1,2)}_\nu (ka) \sim -(2/ka)^{\frac{2}{3}} w'_{1,2}(t) \tag{4}$$

where

$$w_{1,2}(t) = Ai(t) \mp i Bi(t), \qquad \nu = ka + (ka/2)^{\frac{1}{3}} t \tag{4a}$$

The resonance equation for the first $\overline{M}$ whispering gallery modes bound most closely to the impedance surface is then approximated by

$$Ai'(t_m) + i\alpha Ai(t_m) = 0, \quad m = 1, 2, \ldots, \overline{M}, \qquad \alpha = Z'(\frac{ka}{2})^{\frac{1}{3}} \tag{5a}$$

where the t_m are solutions of the differential equation

$$\frac{dt_m}{d\xi} = \frac{1}{t_m - \xi^2} , \qquad \xi = -i\alpha \tag{5b}$$

In the other domain, where $|\nu - ka| > O(|\nu|^{\frac{1}{3}})$, one may employ the Debye approximations

$$J_\nu(ka) \sim \sqrt{\frac{2}{\pi ka \cos w}} \ \sin[\zeta(w) + \pi/4]$$

$$J_\nu'(ka) \sim \sqrt{\frac{2 \cos w}{\pi ka}} \ \cos[\zeta(w) + \pi/4] \tag{6}$$

$$H_\nu^{(1)}{}^{(2)}(ka) \sim \sqrt{\frac{2}{\pi ka \cos w}} \ \exp[\pm i\zeta(w) \mp i\pi/4]$$

$$H_\nu'{}^{(1)}{}^{(2)}(ka) \sim \sqrt{\frac{2 \cos w}{\pi ka}} \ \exp[\pm i\zeta(w) \pm i\pi/4]$$

with

$$\zeta(w) = ka[\cos w - (\pi/2 - w)\sin w], \quad \nu = ka \sin w, \quad \text{Re } w > 0 \tag{6a}$$

to obtain the resonance equation

$$\cos w_m \cos[\zeta(w_m) + \pi/4] - iZ' \sin[\zeta(w_m) + \pi/4] = 0, \quad m = \overline{M} + 1, \ldots M_1 \tag{7}$$

It is found that the two approximations in (5a) and (7) have an operlapping domain wherein one may switch from one to the other. For the case in Fig. 2, $\overline{M} = 4$ has been found satisfactory.

B. Whispering Gallery (W.G.) Mode and Continuous Spectrum Representation

When the contour C in Fig. 1 is deformed into a contour extending along the imaginary ν-axis. the Green's function can be represented as a sum of whispering gallery (W.G.) modes G_m and a continuous spectrum R_{M_1}:

$$G = \sum_{m=1}^{M_1} G_m + R_{M_1} \tag{8}$$

where

$$G_m = \frac{J_{\nu_m}(ka) \exp[i\nu_m|\phi-\phi'|+i\pi/2]}{ka(\partial/\partial\nu)\{J_\nu'(ka)-iZ'J_\nu(ka)\}} \bigg|_{\nu=\nu_m} \tag{9}$$

with the ν_m satisfying the resonance equation in (3). In obtaining the residue contributions in (9) due to the poles at ν_m, the Wronskian relation

$$\frac{1}{i\pi ka[H_\nu'^{(2)}(ka)-iZ'H_\nu^{(2)}(ka)][J_\nu'(ka)-iZ'J_\nu(ka)]} = \frac{1}{2}\left[\frac{J_\nu(ka)}{J_\nu'(ka)-iZ'J_\nu(ka)} - \frac{H_\nu^{(2)}(ka)}{H_\nu'^{(2)}(ka)-iZ'H_\nu^{(2)}(ka)}\right] \tag{9a}$$

has been utilized. Using the Fock approximations in (4) and (5), one finds

$$G_m \sim \frac{\exp(iks+i\gamma t_m-i\pi/2)}{2(ka/2)^{\frac{1}{3}}(t_m+\alpha^2)} \quad , \qquad m = 1 \ldots \overline{M} \tag{10}$$

where

$$s = a\left|\phi-\phi'\right| , \qquad \gamma = \left(\frac{ka}{2}\right)^{\frac{1}{3}} \frac{s}{a} \qquad (10a)$$

Here, s denotes the path length between source and observation point along the boundary, and γ is an arc length parameter. For the remaining modes, (6) and (7) may be used to obtain

$$G_m \sim \frac{\exp(iks\sin w_m + i\pi/2)}{ka(\pi/2-w_m)\cos w_m[1-(Z'/\cos w_m)^2]} , \qquad m=\bar{M}+1\ldots M_1 \qquad (11)$$

From the behavior of the roots as discussed in Section A, one can see that the residue contribution arising from the $m=1$ pole singularity at t_1 (the first root of (5)) describes either a whispering gallery mode bound most closely to the impedance boundary or a surface wave mode when $\mathrm{Re}\, t_1 > 0$, $\mathrm{Im}\, t_1 = 0$. In the latter instance, G_1 in (10) becomes a surface wave field. As in the lossless case, the continuous spectrum

$$R_{M_1} = \frac{1}{i(\pi ka)^2} \int_{-i\infty}^{i\infty} \frac{\exp(i\nu\left|\phi-\phi'\right|)}{[J'_\nu(ka)-iZ'J_\nu(ka)][H'^{(2)}_\nu(ka)-iZ'H^{(2)}_\nu(ka)]}\, d\nu \qquad (12)$$

can be approximated by[4]

$$R_{M_1} \sim \frac{1}{\pi} \int_0^\infty \frac{\exp(-ks\sinh v)}{1-(Z'/\cosh v)^2}\, dv \qquad (12a)$$

C. Ray-Optical plus Slow Wave Representation

With a view toward a ray-optical representation, it is convenient to deform the contour C in Fig. 1 into $\bar{C}$, whence G becomes

$$G = \bar{G} + G_1 U(t_1) \qquad (13)$$

where $\overline{G}$ is the same as G except for the replacement of C by $\overline{C}$ in (2), and G_1 is the contribution (if any) from the pole singularity at t_1 located between C and $\overline{C}$. The unit step function $U(t_1)$ contributes only when the t_1 pole lies between the two contours. The extraction of G_1, which may be either a slow wave W.G. mode or a surface wave, is desirable since slow wave fields do not exhibit ray-optical properties.

To convert $\overline{G}$ into ray-optical form, we substitute the traveling wave expansion

$$\frac{1}{J_\nu'(ka)-iZ'J_\nu(ka)} = \frac{2}{H_\nu'^{(2)}(ka)-iZ'H_\nu^{(2)}(ka)} \sum_{n=0}^{\infty} (-r)^n, \quad |r|<1 \qquad (14)$$

$$r = \frac{H_\nu'^{(1)}(ka)-iZ'H_\nu^{(1)}(ka)}{H_\nu'^{(2)}(ka)-iZ'H_\nu^{(2)}(ka)} \qquad (14a)$$

into (2), with G and C replaced by $\overline{G}$ and $\overset{\bullet}{C}$, respectively. Then with the Debye asymptotic formulas in (6), changing variables from ν to w via $\nu = ka \sin w$,

$$\overline{G} = \sum_{n=0}^{\infty} \overline{G}_n \qquad (15)$$

where

$$\overline{G}_n = \frac{(-i)^n}{\pi} \int_{C_n'} \frac{\cos^2 w}{(\cos w + Z')^2} \cdot \left(\frac{\cos w - Z'}{\cos w + Z'}\right)^n e^{ikaq_n(w)} \, dw \qquad (15a)$$

and

$$q_n(w) = |\phi-\phi'|\sin w + 2(n+1)[\cos w - (\pi/2 - w)\sin w] \qquad (15b)$$

The integral in (15a) can be evaluated in terms of the contributions from the saddle points w_{sn} and $\overline{w}_s$ of $q_n(w)$, determined from the condition $dq_n/dw=0$:

$$w_{sn} = \frac{\pi}{2} - \frac{|\phi-\phi'|}{2(n+1)}, \qquad \overline{w}_s = \frac{\pi}{2} \qquad (16)$$

A typical path C_n' passing through the n-th saddle point is shown in Fig. 3 (note that the whispering gallery mode poles w_m have been eliminated from the integrand in (15a)). Upon using the conventional saddle point formula (ref. 2, p. 382) one finds

$$\bar{G}_n \sim e^{i\pi/4} \sqrt{\frac{2}{\pi k}} (-i)^n \frac{(\Gamma_n)^n \cos^2 w_{sn} \exp(ikD_n)}{(\cos w_{sn} + Z')^2 \sqrt{D_n}} \tag{17}$$

where

$$D_n = 2(n+1) a \sin [|\phi-\phi'|/2(n+1)] \tag{17a}$$

and Γ_n is the boundary reflection coefficient for ray species n,

$$\Gamma_n = \frac{\cos w_{sn} - Z'}{\cos w_{sn} + Z'} \tag{17b}$$

The expression in (17) corresponds to a geometric-optical ray field that has undergone n reflections at the impedance boundary (see Fig. 4). The sum in (15) can actually not be extended to $n \to \infty$ since the Debye approximations in (6) become invalid as $w_{sn} \to \pi/2$. This situation arises either when the observation point approaches the source point so that $|\phi-\phi'| \to 0$, or when the number of rays increases, with $|\phi-\phi'|$ fixed. The latter case can be avoided by truncating the number of rays at some $n = N$ such that w_{sN} is sufficiently less than $\pi/2$ (see Sec. D) while the former case will be discussed in Section F.

D. Ray plus Canonical Integral plus Slow Wave Representation

When instead of (14) the partial expansion

$$\frac{1}{J_\nu'(ka) - iZ'J_\nu(ka)} = \frac{2}{H_\nu'^{(2)}(ka) - iZ'H_\nu^{(2)}(ka)} \sum_{n=0}^{N} (-r)^n + \frac{(-r)^{N+1}}{J_\nu'(ka) - iZ'J_\nu(ka)} \tag{18}$$

is substituted into (2) (with G and C replaced by $\bar{G}$ and $\bar{C}$, respectively), one has instead of (13) and (15)

$$G = \sum_{n=0}^{N} \bar{G}_n + R_N + G_1 U(t_1) \tag{19}$$

where

$$R_N = \frac{1}{i(\pi ka)^2} \int_{\bar{C}} \frac{(-r)^{N+1} \exp(i\nu |\phi - \phi'|)}{[H_\nu'^{(2)}(ka) - iZ'H_\nu^{(2)}(ka)][J_\nu'(ka) - iZ'J_\nu(ka)]} d\nu \tag{19a}$$

$\bar{G}_n$, given in (17), again describes a geometrical ray field having undergone n reflections. The remainder term R_N accounts for ray fields reflected more than N times.

One way of dealing with (19a) is to investigate how fast the integrand decays in the neighborhood of the point $\nu = ka$; rapid decay permits effective truncation of the integration path and the use of further approximations. Proceding as in the $Z' = 0$ case,[1] one may show that the main contribution to the integral arises from the neighborhood of $\nu = ka$ provided that the arc length parameter γ defined in (10a) and the number of rays (N+1) satisfy the left-hand portion of the inequality

$$\frac{\gamma}{2(2^3\Delta)^{\frac{1}{2}}} - 1 < (N+1) < \frac{\gamma}{2(2^3\Delta)^{\frac{1}{2}}} . \tag{20}$$

where $\Delta = \Delta(ka, Z') = O(1)$ and $|Z'| \ll 1$. The right-hand portion of the inequality validates use of the Debye approximations in the first term on the right-hand side of (18), which has been used to derive $\bar{G}_n$ in (17). The complete inequality in (20) provides a criterion for the number of geometric optical ray fields that are identified in (19). The precise choice of Δ is not too important; a value $\Delta \approx 2$ has been found adequate in our various numerical comparisons[1] (Sec. III).

Since the contributing portion of the integrand in (19a) is localized near $\nu = ka$, one may substitute the asymptotic approximations (4) to obtain

$$R_N \sim \frac{(-1)^{N+1} \exp(iks)}{2i\pi^2 ka} \left(\frac{ka}{2}\right)^{\frac{2}{3}} I_N(\gamma, \alpha), \qquad \alpha = Z'\left(\frac{ka}{2}\right)^{\frac{1}{3}} \tag{21}$$

Here, $I_N(\gamma, \alpha)$ is the canonical integral

$$I_N(\gamma, \alpha) = \int_{C_t} \frac{[\{w_1'(t) + i\alpha w_1(t)\}/\{w_2'(t) + i\alpha w_2(t)\}]^{N+1}}{[w_2'(t) + i\alpha w_2(t)][Ai'(t) + i\alpha Ai(t)]} \, e^{i\gamma t} dt \tag{22}$$

with the path C_t in the complex t plane obtained from C in the complex ν-plane by the shift implied in (4a). The canonical integral in (22) has been evaluated for relevant ranges of γ and three values of α. The results are shown in Fig. 11 and have been tabulated[5]. The canonical integral for a related boundary value problem corresponding to a different integrand and to $\alpha = 0$ has been tabulated by Babich and Buldyrev.[6]

E. Ray plus Whispering Gallery (W. G.) Mode plus Slow Wave Respresentation

An alternative way of treating (19a) is to deform the contour $\overline{C}$ into C_N in Fig. 3 and thereby representing R_N as a sum of $[M-U(t_1)]$ W. G. modes whose poles lie between $\overline{C}$ and C_N, plus some other remainder term R_{MN}. Referring to (9a), one finds

$$R_N = \sum_{m=\overline{m}}^{M} G_m + R_{MN}, \qquad \overline{m} = 1 + U(t_1) \tag{23}$$

where

$$R_{MN} = \frac{1}{2\pi ka} \int_{C_N} \left[\frac{J_\nu(ka)}{J_\nu'(ka) - iZ'J_\nu(ka)} - \frac{H_\nu^{(2)}(ka)}{H_\nu'^{(2)}(ka) - iZ'H_\nu^{(2)}(ka)} \right] (-r)^{N+1} e^{i\nu|\phi-\phi'|} d\nu \tag{24}$$

The sum in (23), with G_m given in (10) or (11), describes W. G. mode contributions.

The evaluation of R_{MN} in (24) may proceed by the saddle point technique, after replacement of the cylinder functions by their Debye approximations as in (6). The integral then becomes:

$$R_{MN} \sim \frac{(-i)^{N+1}}{2\pi} \int_{C_N} \left[\frac{\cos w \tan\{\zeta(w) + \pi/4\}}{\cos w - iZ' \tan\{\zeta(w) + \pi/4\}} - \frac{i \cos w}{\cos w + Z'} \right] \left(\frac{\cos w - Z'}{\cos w + Z'} \right)^{N+1} e^{ikaq_N(w)} dw \tag{25}$$

where $\zeta(w)$ is given in (6a) and $q_N(w)$ in (15b). For observation points such that the saddle point w_{sN} of (25) is located far from the pole singularities of the integrand, and for a low loss impedance, the contribution from the first term inside the square brackets in (25) is negligible when compared with that from the second term. Then from a comparison of (25) with (15a) and (17)

$$R_{MN} \sim -\frac{1}{2} \bar{G}_N \left(1 - \frac{Z'}{\cos w_{sN}} \right) \tag{26}$$

Thus

$$G \sim \sum_{n=0}^{N} \bar{G}_n + \sum_{m=\bar{m}}^{M} G_m - \frac{1}{2} \bar{G}_N \left(1 - \frac{Z'}{\cos w_{sN}} \right) \tag{27}$$

F. Near Field Form

As observed at the end of Section C (see also (20)), any Green's function representation that includes geometric optical terms fails in the near field where the arc length parameter γ in (10a) is less than $2(2^{\frac{1}{3}} \Delta)^{\frac{1}{2}}$. We therefore go back to the basic integral representation in (2). Since the main contribution to the integral arises from the vicinity of $\nu = ka$, the cylinder functions may be replaced by their Fock approximations in (4). Then using the Wronskian relation for the Airy functions (analogous to (9a)) and applying Cauchy's theorem in the upper half of the complex t-plane, one finds

$$G \sim \frac{-\exp(iks)}{2\pi ka} \left(\frac{ka}{2}\right)^{\frac{2}{3}} \int_{-\infty-i\delta}^{+\infty-i\delta} \frac{Ai(t)\exp(i\gamma t)}{Ai'(t) + i\alpha Ai(t)} \, dt \qquad \cdot \qquad (28)$$

Employing large argument expansions for the Airy functions, one may generate an asymptotic expansion of the integrand in (28):

$$- \frac{Ai(t)}{Ai'(t) + \alpha Ai(t)} \sim \sum_{j=0}^{21} \frac{a_j}{t^{(j+1)/2}} + O(t^{-23/2}) \qquad (29)$$

where all of the terms retained (i.e., up to $j = 21$) were employed in subsequent numerical calculations. The coefficients $a_o, a_1, \ldots, a_{21}$ are given by

$$a_j = \begin{cases} \sum_{\ell=0}^{L} d_{j,\ell}(i\alpha)^{3\ell} & , \quad j = 3\ell \\[2ex] \sum_{\ell=0}^{L} d_{j,\ell}(i\alpha)^{3\ell+1} & , \quad j = 3\ell+1 \\[2ex] \sum_{\ell=0}^{L} d_{j,\ell}(i\alpha)^{3\ell+2} & , \quad j = 3\ell+2 \end{cases}$$

where

$$d_{j,L} = 1 \quad , \qquad d_{j,L-1} = -(j-2)/4 \quad , \qquad d_{6,0} = 7/32$$

$$d_{j,L-2} = d_{j-1,L-2} + 9/32 + 2(j-7)/32, \text{ for } j = 3L+1, \ 3L+2, \ (L \geq 2)$$

$$d_{j,L-2} = d_{j-1,L-3} + 9/32 + 2(j-7)/32, \text{ for } j = 3L \ (L \geq 3)$$

$$d_{9,0} = -21/64 \qquad d_{10,0} = -49/64 \qquad d_{11,0} = -85/64$$

$$d_{12,0} = 0.71435 \qquad d_{12,1} = -130/64 \qquad d_{13,0} = 1.64062$$

$$d_{13,1} = -185/64 \qquad d_{14,0} = 2.811982 \qquad d_{14,1} = -251/64$$

$$d_{15,0} = -2.07128 \qquad d_{15,1} = 4.29687 \qquad d_{15,2} = -329/64$$

$$d_{16,0} = -4.64329 \qquad d_{16,1} = 6.12059 \qquad d_{16,2} = -420/64 \qquad (29a)$$

$$d_{17,0} = -7.81345 \qquad d_{17,1} = 8.34373 \qquad d_{17,2} = -525/64$$

$$d_{18,0} = 7.55725 \qquad d_{18,1} = 11.69283 \qquad d_{18,2} = 11.02293$$

$$d_{18,3} = -645/64 \qquad d_{19,0} = 16.57034 \qquad d_{19,1} = -16.4017$$

$$d_{19,2} = 14.21873 \qquad d_{19,3} = -781/64 \qquad d_{20,0} = 27.29129$$

$$d_{20,1} = -22.09779 \qquad d_{20,2} = 17.99556 \qquad d_{20,3} = -934/64$$

$$d_{21,0} = -33.32008 \qquad d_{21,1} = 40.01068 \qquad d_{21,2} = -28.92270$$

$$d_{21,3} = 22.42181 \qquad d_{21,4} = -1105/64$$

Then by Laplace inversion of (28),[7] with (29),

$$G \sim \frac{e^{iks+i\pi/4}}{\sqrt{2\pi k s}} \left\{ 1 + \sum_{j=1}^{21} b_j \gamma^{j/2} + O(\gamma^{11}) \right\} , \quad |a| \leq 1 \tag{30}$$

where

$$b_j = \begin{cases} \sqrt{\pi} \; a_j \; e^{i(\frac{\pi}{4}j)} \Big/ \left(\frac{j-1}{2}\right)! & , \; j \; \text{odd} \\[2em] 2^{j/2} a_j \; e^{i(\frac{\pi}{4}j)} \Big/ \prod_{m=1}^{j/2} (2m-1), & j \; \text{even} \end{cases} \tag{30a}$$

The restriction $|a| \leq 1$ in (30) arises from the condition $\left| a \, Ai(t)/Ai'(t) \right| < 1$, required for validity of the expansion in (29). In view of the definition of α in (5a), the solution (30) can therefore not be applied to the infinite plane limit $a \to \infty$ if Z' differs from zero.

III. Numerical Results

Extensive numerical computations have been performed for $ka = 100$ and for various surface impedance values to show how the amplitude and phase of the surface impedance affect the field, and to check the accuracy and range of validity of the various formulations in Section II.

Concerning the propagation constants for the W. G. modes, we have obtained solutions of the differential equation (5b) by the Runge-Kutta method. The results are shown in Fig. 5. Here t_1, t_2 and t_3 are the first three roots of $Ai'(t_m) = 0$ (i. e., $\alpha = 0$ in (5a)) and $\tilde{t}_1$, $\tilde{t}_2$ and $\tilde{t}_3$ are those of $Ai(\tilde{t}_m) = 0$ (i. e., $\alpha = \infty$ in (5a)). The solid lines and the dotted lines are equi-phase and equi-amplitude curves, respectively. The arrows on the equi-phase curves indicate the directions along the root loci with increasing amplitude $|\xi|$. It is interesting to note in Fig. 5 that the first zero t_1 crosses the imaginary axis for some values of ξ, thereby furnishing the slow wave type of whispering gallery mode. In particular, when $Re\ t_1 > 0$, $Im\ t_1 = 0$, the contribution from t_1 describes a surface wave mode. Except for $arg\ Z' = \pm\ 90°$, the imaginary parts of the whispering gallery mode poles become large as the amplitude of Z' increases within the ranges under consideration (i. e., $|Z'| < 0.6$). It should be noted in Figs. 2 and 5 that, for given Z' and $arg\ Z' \neq \pm\ 90°$, the eigenvalues for modes bound close to the surface have large imaginary parts compared to those located far from the surface, thereby de-emphasizing the importance of the most closely bound whispering gallery modes. This is to be expected on physical grounds since the field of the tightly bound modes is in close proximity to the lossy guiding surface. It can also be seen from Fig. 2 that the two approximations given in (5a) and (7) have an overlapping region wherein one can switch from one to the other. $\overline{M} = 4$ has been found

satisfactory for our evaluation of the field.

In Figs. 6-7, we have compared the various formulations in Section II for a purely inductive impedance case ($|Z'| = 0.22$ and arg $Z' = -90^\circ$) to check accuracy and range of validity. For this case, the surface wave mode is excited since the first root of (5a) or (5b) is located on the positive real axis in the t-plane. The ray plus canonical integral plus slow wave representation in (19) is seen to provide an excellent approximation provided that the number of rays (N+1) is chosen according to the criterion in (20). Because of the overlap of the curves for various N, switching from one formulation to the other can be performed smoothly. The ray plus canonical integral contribution curves are shown separately to exhibit the effect of the surface wave on the total field.

In Fig. 7, the near field form in (30) and the ray plus whispering gallery mode plus slow wave representation in (27) are compared with the whispering gallery mode (including surface wave) plus continuous spectrum representation in (8). It is interesting to observe that for large enough γ, the total field can be accurately represented just by the surface wave (M=1) and by rays provided that the appropriate number of reflected rays is included as γ or $|\phi - \phi'|$ increases.

Curves for a high loss case are depicted in Figs. 8(a) and 8(b), based on the ray plus canonical integral representation and on the ray-optical representation, respectively, with the latter implying omission of the canonical integral contribution. Having in mind an application to ground wave propagation, the high loss impedance $Z' = 0.22 \exp(-i30.5^\circ)$ has been obtained by assuming a wet ground surface with conductivity $\sigma_e = 10^{-2}$ mho m^{-1} and dielectric constant $\epsilon_e = 10 \epsilon_o$, subject to a wave frequency f = 10MHz. Also shown in Fig. 8(b) is the near field form for small γ. It should be noted that G_1 in (19) does not

contribute since no pole singularity is located between the contours C and
$\overline{C}$ in Fig. 1 (see also Section II-A).   All of the modes here are fast waves
as seen from Fig. 2.   Note that the ray-optical contribution alone is adequate
for describing the field sufficiently far from the source point because of the
dissipative attenuation of the modes bound close to the surface, as mentioned
previously.

The solid curves in Figs. 6-8 are obtained from (8) with
$M_1 = 32$(ka=100).   This form of the solution is taken as a reference for all
γ.   It was noted in the study of the perfect conductor case[1] that the
numerical values derived from the W.G. mode plus continuous spectrum
representation are extremely sensitive to the exact number of modes re-
quired.   Unless all 32 modes (for ka=100) are included, the perfect con-
ductor curve was found to deviate appreciably from the correct shape.   The
same remark applies to the finite surface impedance case in Figs. 6-8
since the higher order modes have small attenuation coefficients (see Fig. 2)
even though the losses may be large.   Because of this feature, it is pre-
ferable to use one of the other representations for field calculation.

In Figs. 9(a)-(e), we have shown, for given phase of the normalized
impedance Z', how increasing the amplitude of Z' affects the surface
field.   Curves are depicted based on the ray plus canonical integral plus
slow wave (if necessary) representation, and on the near field form for
small γ.   In our computations, $|Z'| = 0.05$ has been chosen as a sample of
a small impedance, and $|Z'| = 0.22$ as a sample of a large impedance.   If
arg Z' = -90°, corresponding to a purely inductive impedance boundary, the
field amplitude increases as $|Z'|$ increases (see Fig. 9(a)) while the con-
verse is true when the boundary impedance is purely capacitive (see
Fig. 9 (e)).   This behavior may be attributed to the greater and lesser

confinement, respectively, of the lowest order modal field in the two cases. As the imaginary part of roots increases (see Fig. 4),the field transmitted to an observation point tends to decrease (Figs. 9(b)-(d)). Because of the absorption on the surface, the interference effects between rays are also weakened, as seen from the decreasing magnitude of oscillation in the curves in Figs. 9(b)-(d).

The curves in Fig. 10 show the effect of the phase of Z' on the field when the amplitude remains constant at $|Z'| \cong 0.05$. One observes that the field tends to increase as the phase of Z' deviates from zero; this could have been predicted from the behavior of poles in Fig. 5. Note that the maxima and minima of the field shift backward for negative phase (i.e., $-90^{\circ} \leq \arg Z' < 0^{\circ}$) and forward for positive phase (i.e., $0^{\circ} < \arg Z' \leq 90^{\circ}$).

IV. Conclusions

A variety of alternative representations have been explored in this study of the surface fields excited by a line source located on a concave cylindrical impedance boundary. As for the previously investigated perfectly conducting case[1], these different formulations provide new insights into the propagation mechanisms that prevail for various parameter ranges involving the boundary shape, separation of source and observation points, and the surface impedance. From the detailed discussion and interpretation of the numerical results in Section III emerges the role played by the geometric optical field and, for sufficiently inductive boundaries, by the surface wave. The presence of the surface wave leads to an enhancement of the field over that observed on a perfect conductor. When losses are appreciable, attenuation of mode fields bound close to the boundary establishes the geometric optical field as the dominant and adequate constituent. The versatility of representations involving the canonical integral has again been confirmed, and tabulations have been provided for several values of surface impedance.

REFERENCES

1. T. Ishihara, L.B. Felsen, and A. Green, "High Frequency Fields Excited by a Line Source Located on a Perfectly Conductiong Concave Cylindrical Surface," to be published in IEEE Transactions on Antennas and Propagation.

2. L.B. Felsen, and N. Marcuvitz, Radiation and Scattering of Waves. Englewood Cliffs, N.J.: Prentice Hall, Inc., Secs. 2.3, 3.4, 1973.

3. V.M. Babich, and V.S. Buldyrev, Asymptotic Methods of Short Wave Diffraction, Moscow, USSR: Nauka, Chapter 11, Section 4 1972.

4. W. Wasylkiwskyj, "Exact and Quase-Optic Diffraction within a Concave Cylinder," IEEE Transactions on Antennas and Propagation, Vol. AP-23, No. 4, p. 480-492, 1975.

5. T. Ishihara, "Tabulation of a Canonical Integral Occurring in the Theory of Wave Propagation Along a Concave Cylindrical Impedance Surface", submitted for publication

6. V.M. Babich, and V.S. Buldyrev, Aymptotic Methods of Short Wave Diffraction, Moscow, USSR: Nauka, Appendix 4, 1972.

7. G. Hasserjian, and A. Ishimaru, "Currents Inducted on the Surface of a Conducting Circular Cylinder by a Slot," J. Res. Nat.Bur. Stand., Vol. 66D, No. 3, p. 335-365, 1972.

FIGURE CAPTIONS

FIG. 1   Integration path and singularities in complex ν-plane.
xx--zeros ν_p of $[H'^{(2)}_\nu(ka) - iZ'H^{(2)}_\nu(ka)]$; ●● -- zeros ν_m of
$[J'_\nu(ka) - iZ'J_\nu(ka)]$.

FIG. 2   Zeros of $[J'_\nu(ka) - iZ'J_\nu(ka)]$ in complex w-plane.
●●--zeros for $Z'= 0$ (perfect conductor); oo-- zeros for $Z'= 0.05 \exp(-i30.5^\circ)$
(small loss); ꓱꓱ --, ▲▲ -- zeros for $Z' = 0.22 \exp(-i30.5^\circ)$
(large loss).   The first five roots ▲▲ -- are obtained from (5b)
and compared with ▣▣ -- obtained from (7).

FIG. 3   Disposition of integration paths

FIG. 3(a)   Steepest descent paths in complex ν-plane

FIG. 3(b)   Steepest descent paths in complex w-plane ($\nu = ka \sin w$)

FIG. 4   Direct and multiply reflected rays for a circular boundary.
Geometrical quantities D_0, D_1, D_2, w_{s0}, w_{s1} and w_{s2} are also
shown.

FIG. 5   Roots of $[Ai'(t_m) + i\alpha Ai(t_m)]$ as obtained from (5b).   The
numbers on the solid and dashed curves denote the phase and
amplitude of $\xi = -i\alpha$, respectively.

FIG. 6   Ray plus canonical integral plus slow wave representation in
(19), with $Z'= 0.22 \exp(-i90^\circ)$.   Both the γ and $|\phi-\phi'|$
coordinates are indicated.   Also shown are the ranges in γ and
$|\phi-\phi'|$ corresponding to $N = -1$ (—●—●—) (no geometric-optical
ray); $N = 0$ (—·—)(1 ray); $N = 1$ (—·—·—)(2 rays); $N = 2$ (—··—)
(3 rays).   The solid curve is calculated from (8) and serves as
the reference solution.   The heavy curves include the surface
wave in (19) ($U(t_1) = 1$ for this case), while the light curves have
been obtained from (19) with the surface wave omitted.

FIG. 7   Ray plus W.G. mode plus slow wave representation in (27), and near field form in (30) (--), with $Z' = 0.22 \exp(-i90^\circ)$. The reference solution (solid curve) is calculated from (8). The numbers indicated along the curves should be read as follows: for example, $M = 2$ $[N=1]$ denotes the range wherein the direct ray and singly reflected rays plus 2 modes (1 W.G. mode and 1 surface wave mode) are applicable, while the circles indicate the starting point of the relevant intervals. The $|\phi - \phi'|$ coordinate is not shown since it has been depicted in Fig. 6.

FIG. 8   Ray plus canonical integral representation in (19), and near field form (--) in (30), with $Z' = 0.22 \exp(-i30.5^\circ)$. Note that $U(t_1) = 0$ in this example (see Fig. 2). The reference solution (solid curve) is calculated from (8).

FIG. 8(a)   Canonical integral contribution R_N included, —•—•— $N=-1$; —·— $N = 0$, —··— $N = 1$; —···— $N = 2$.

FIG. 8(b)   Canonical integral contribution R_N' omitted. —··— $N = 1$; —···— $N = 2$.

FIG. 9   Influence of the amplitude of the surface impedance Z', calculated from (19) and (30) (--), for various phase angles. The heavy curves represent a large impedance ($|Z'| = 0.22$) and the light curves a small impedance ($|Z'| = 0.05$). Here, $U(t_1) = 0$ except for the case $Z' = 0.22 \exp(-i90^\circ)$. —•—•— $N = -1$; —·— $N = 0$; —··— $N = 1$; and —···— $N = 2$.

FIG. 9(a) $\arg Z' = -90^\circ$

FIG. 9(b) $\arg Z' = -45^\circ$

FIG. 9(c) $\arg Z' = 0^\circ$

FIG. 9(d) $\arg Z' = 45^\circ$

FIG. 9(e) $\arg Z' = 90^\circ$

FIG. 10   Influence of the phase of the surface impedance Z', calculated from (19), with $|Z'| = 0.05$.

FIG. 10(a)   Negative phase angle.

————— arg $Z' = 0^O$; —·— arg $Z' = -45^O$;

—··— arg $Z' = -90^O$.

FIG. 10(b)   Positive phase angle.

————— arg $Z' = 0^O$; —·—·— arg $Z' = 45^O$;

—●—●— arg $Z' = 90^O$

FIG. 11   Plot of canonical integral $|I_N (\gamma , \alpha)|$ vs. γ .

Solid curves: $Z' = 0$ ($\alpha = 0$) (perfect conductor);

—··—·— $Z' = 0.05 \exp(-i30.5^O)$ or $Re\alpha = 0.16799$,

$Im \alpha = - 0.09903$ (small loss) ; —··—··—

$Z' = 0.22 \exp(-i30.5^O)$ or $Re\alpha = 0.6997$,

$Im \alpha = -0.41261$ (large loss).

FIG.1

FIG.2

ν–Plane

c_n c_N $\overline{c}$

$\nu = ka$
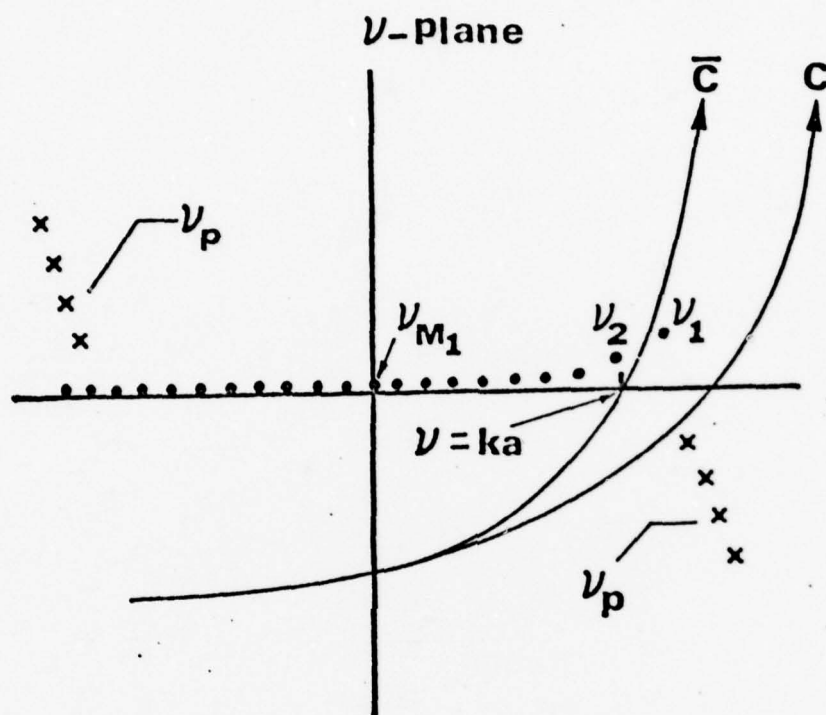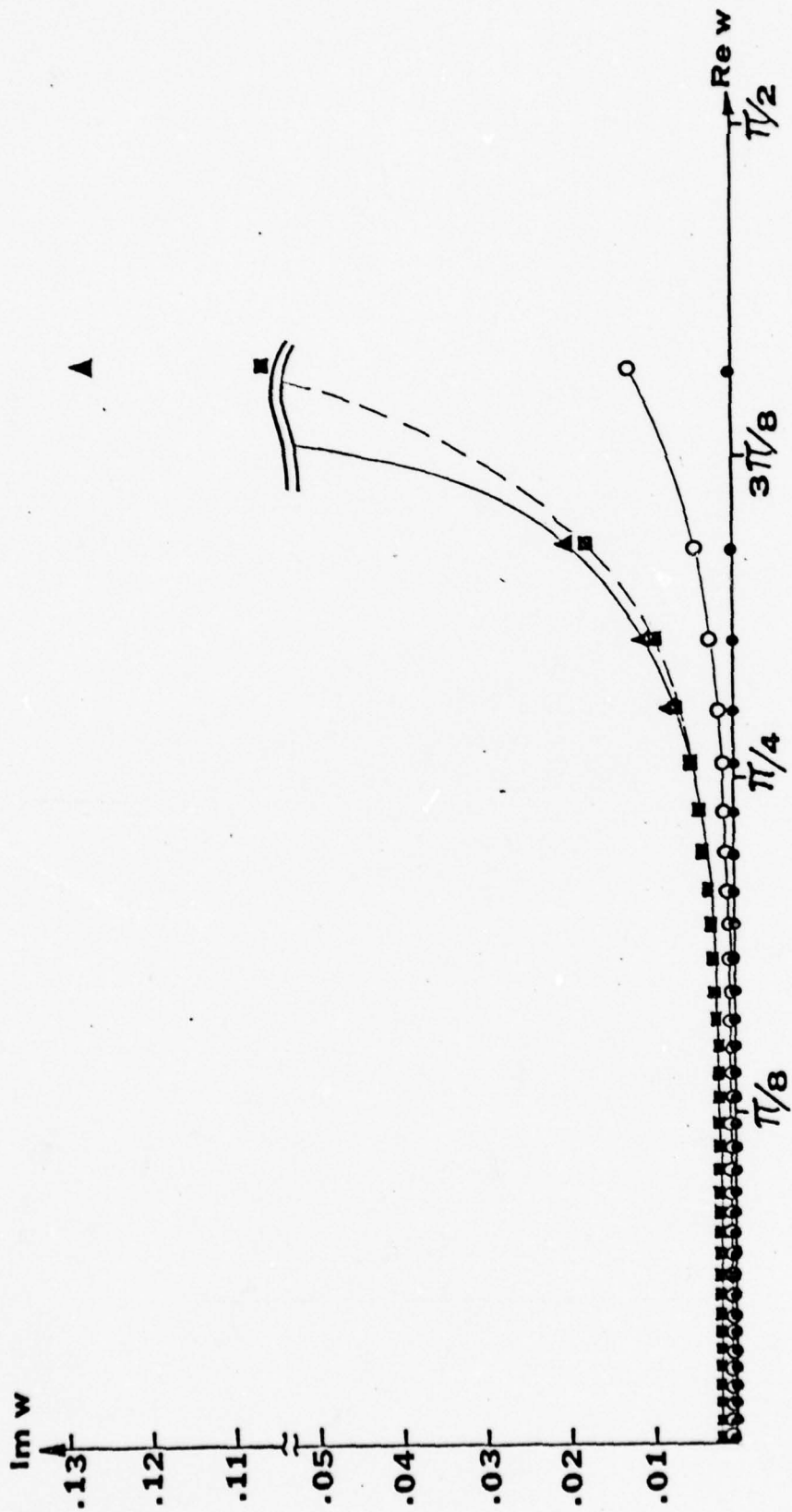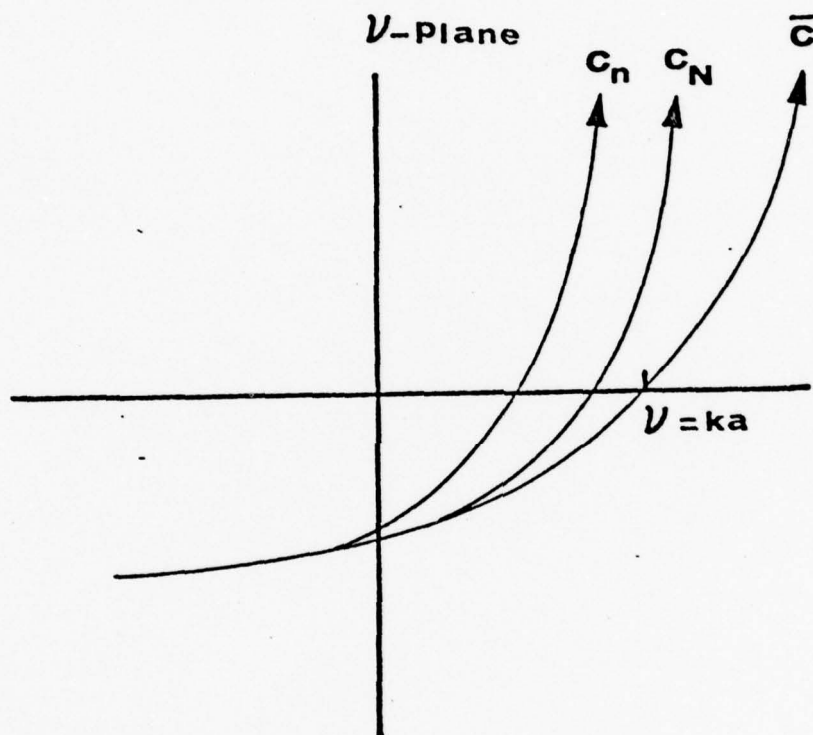
FIG. 3 (a)
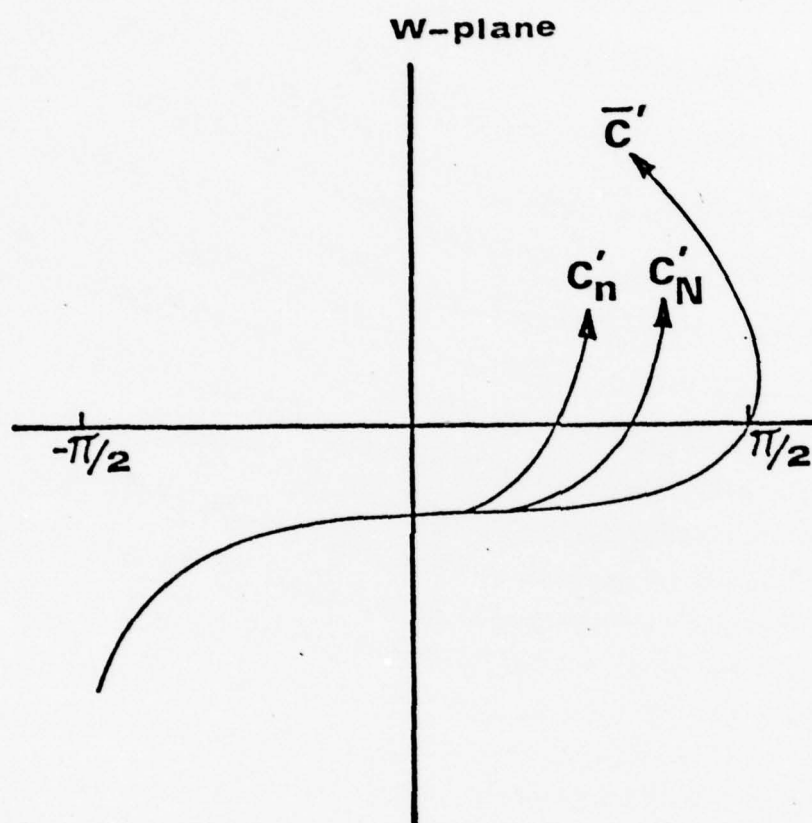
FIG. 3 (b)
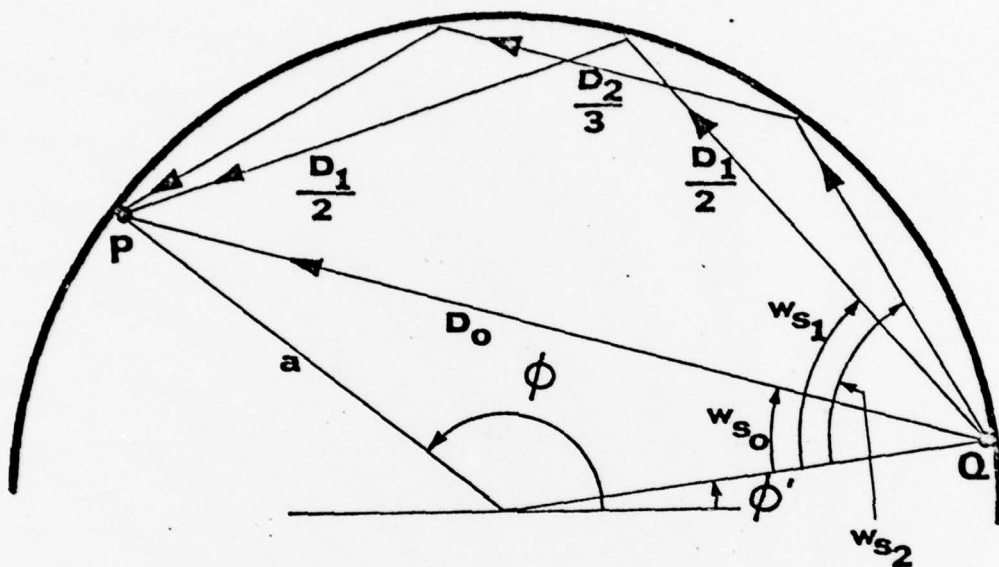
FIG. 4
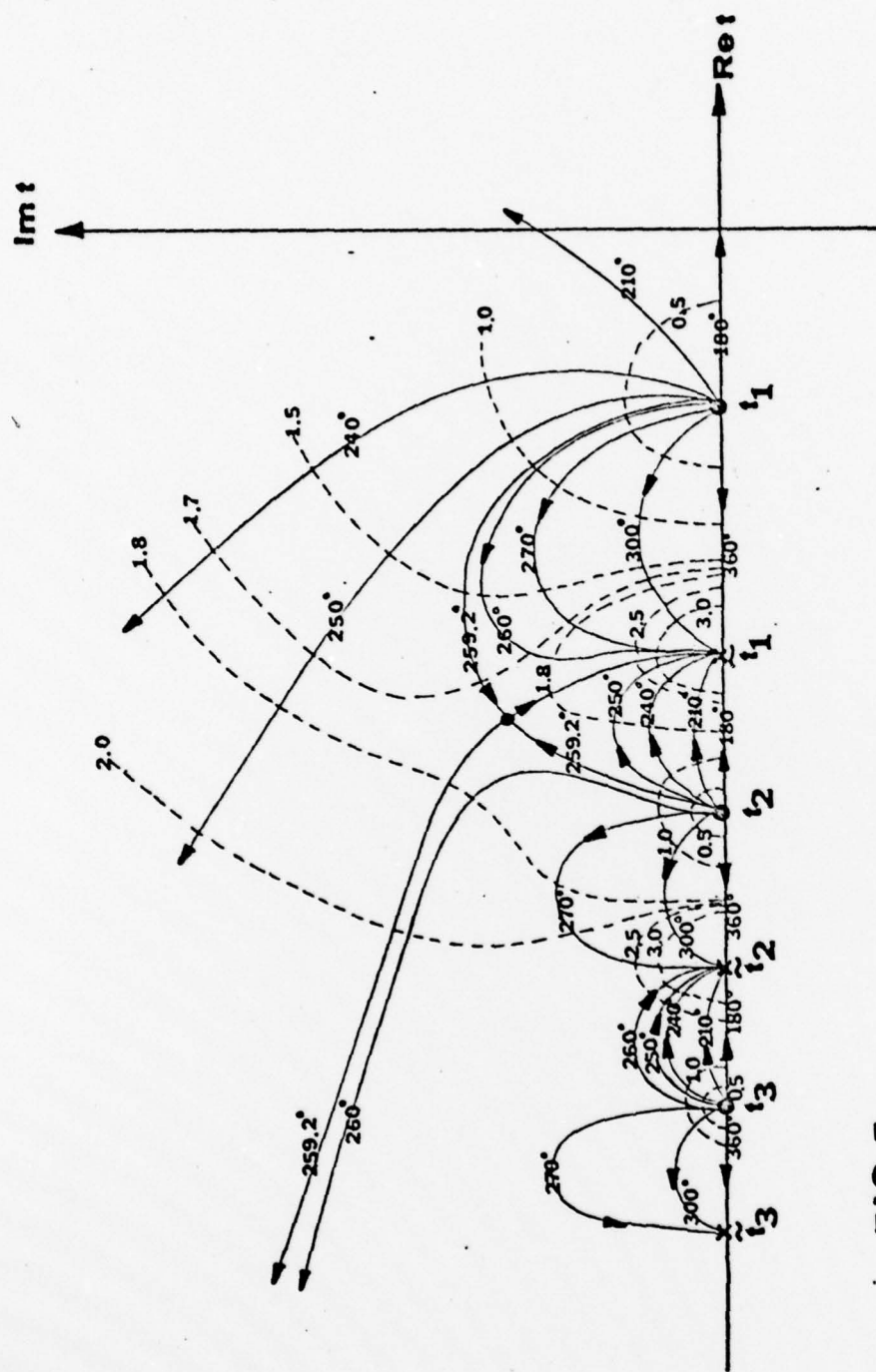
FIG. 5
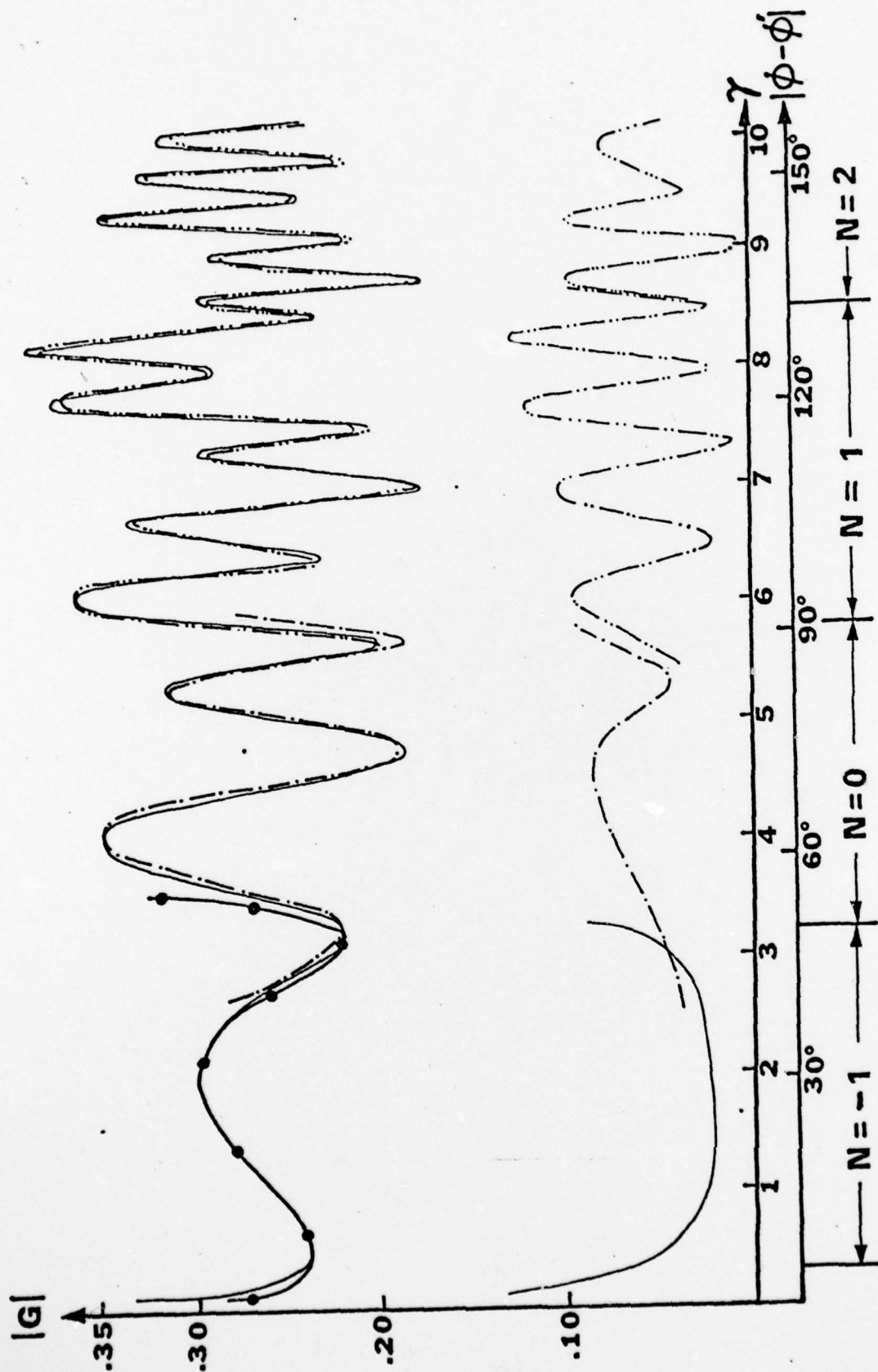
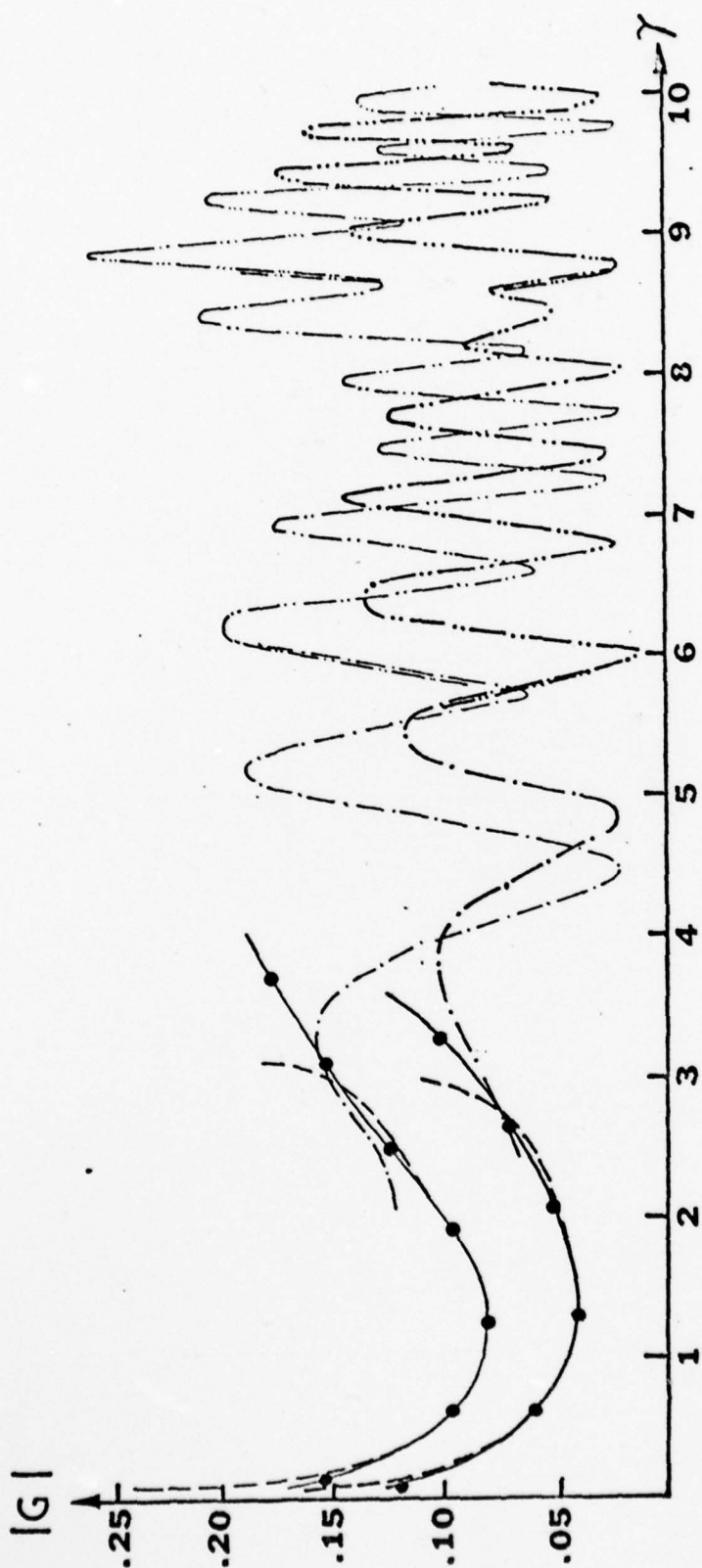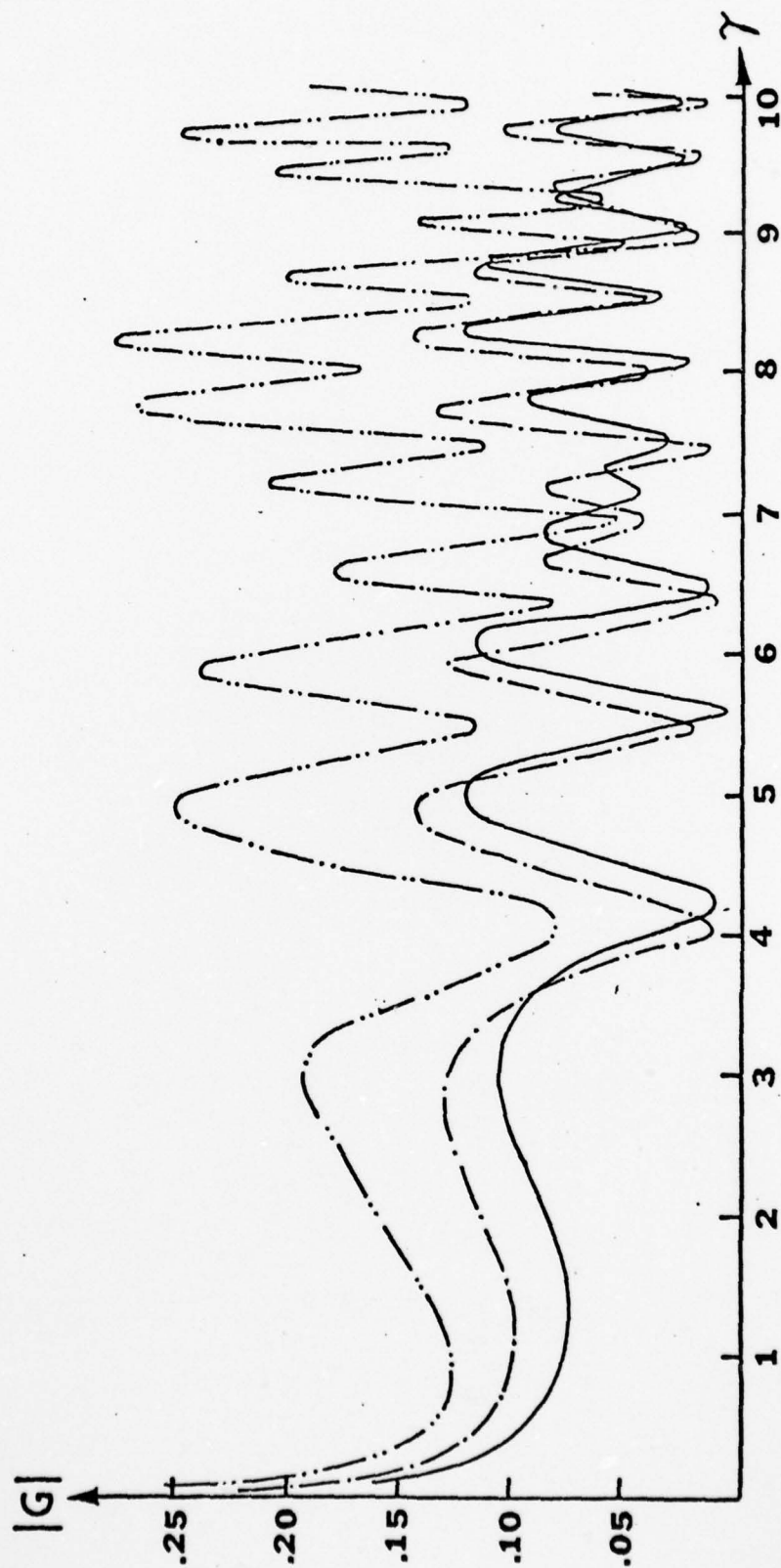FIG. 6
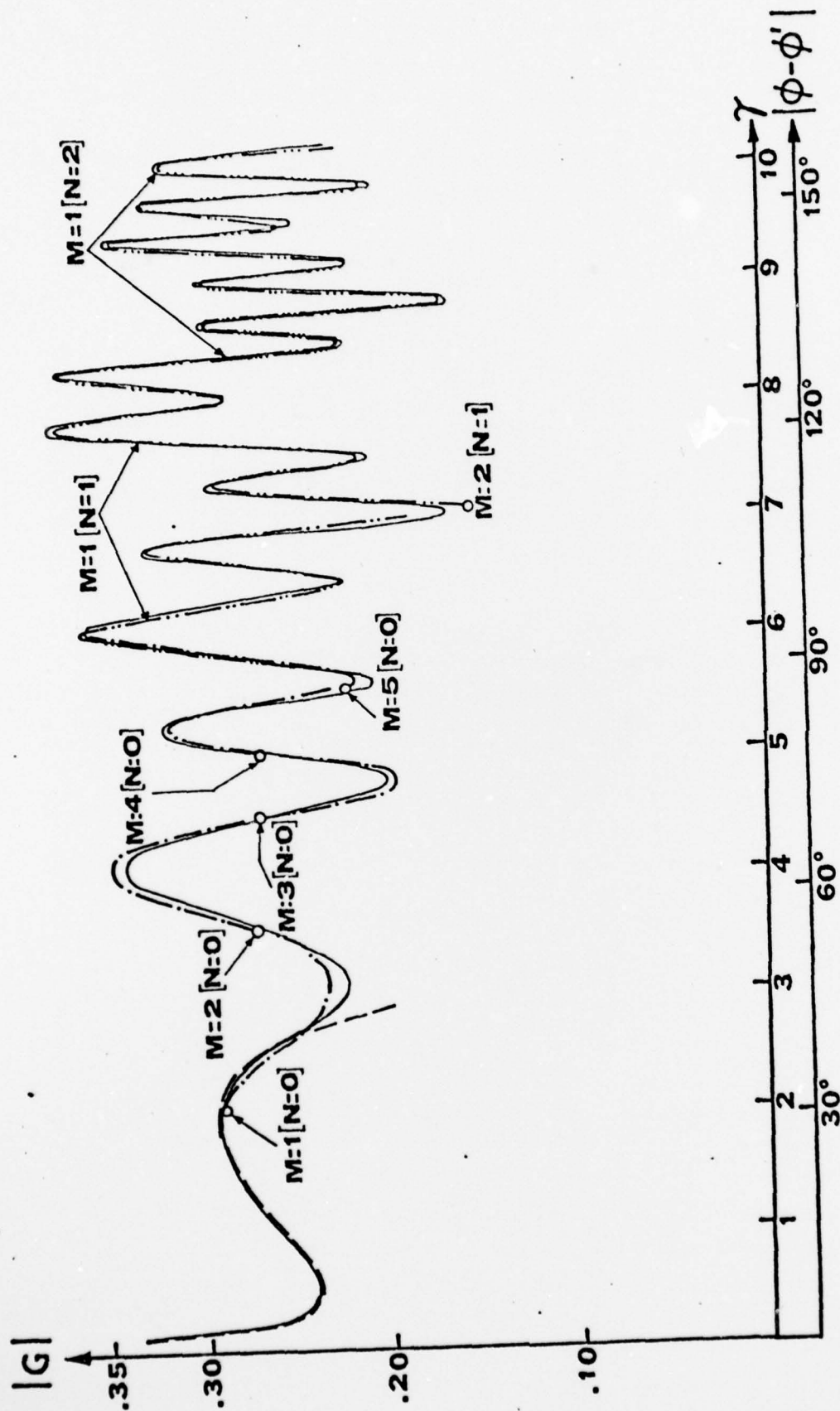
FIG. 7
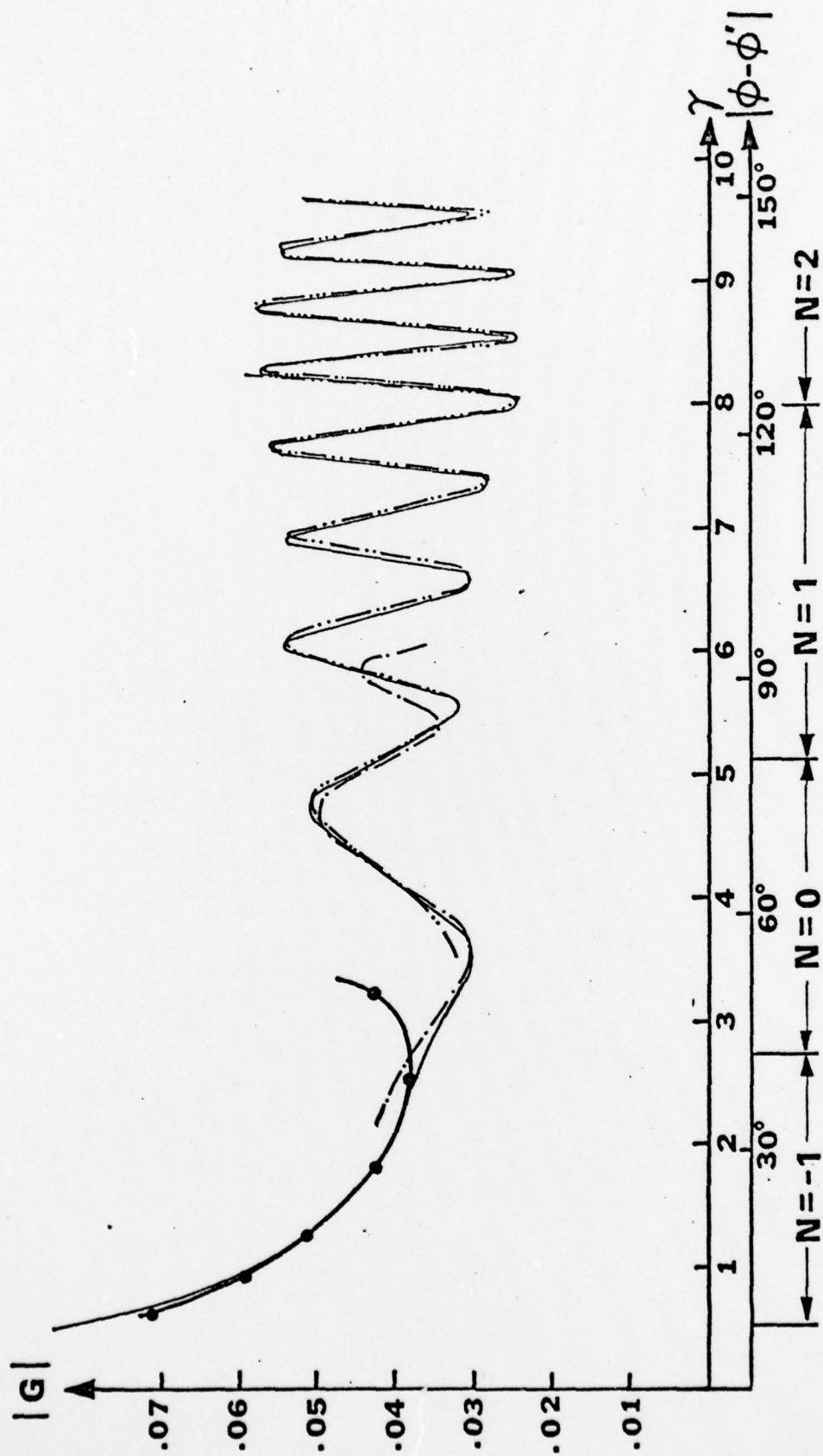
FIG. 8 (a)
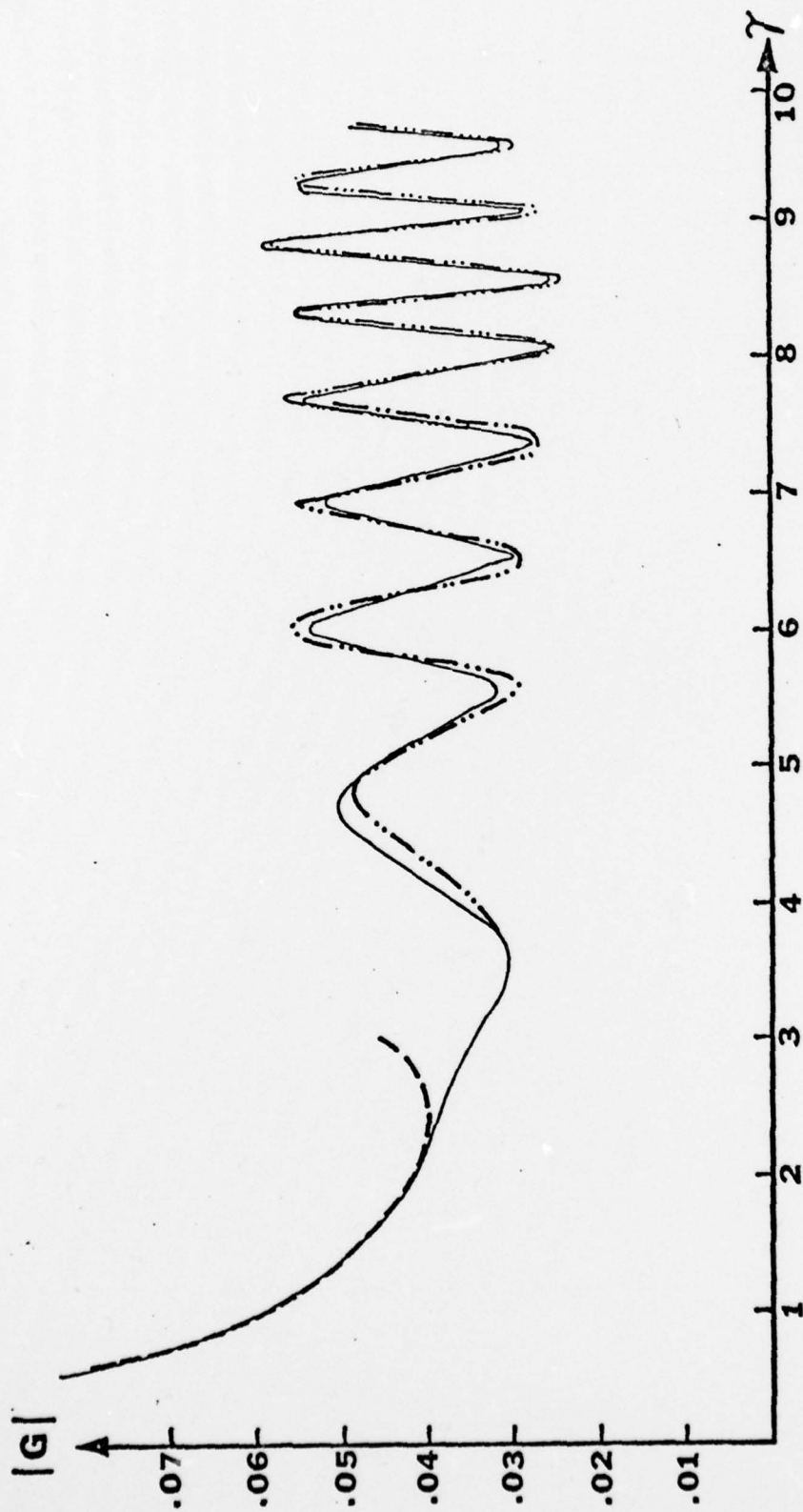
FIG.8 (b)
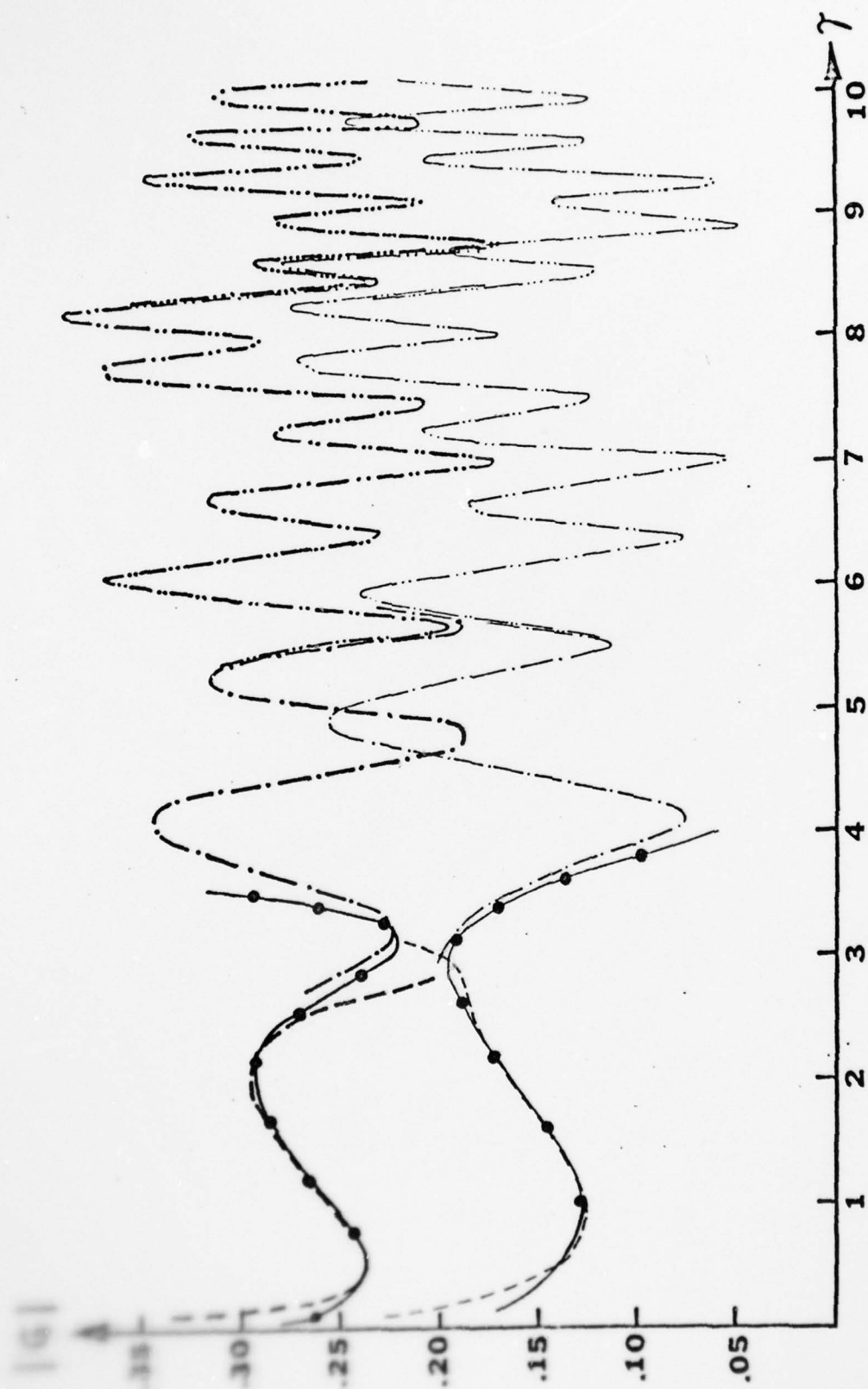
FIG. 9 (a)
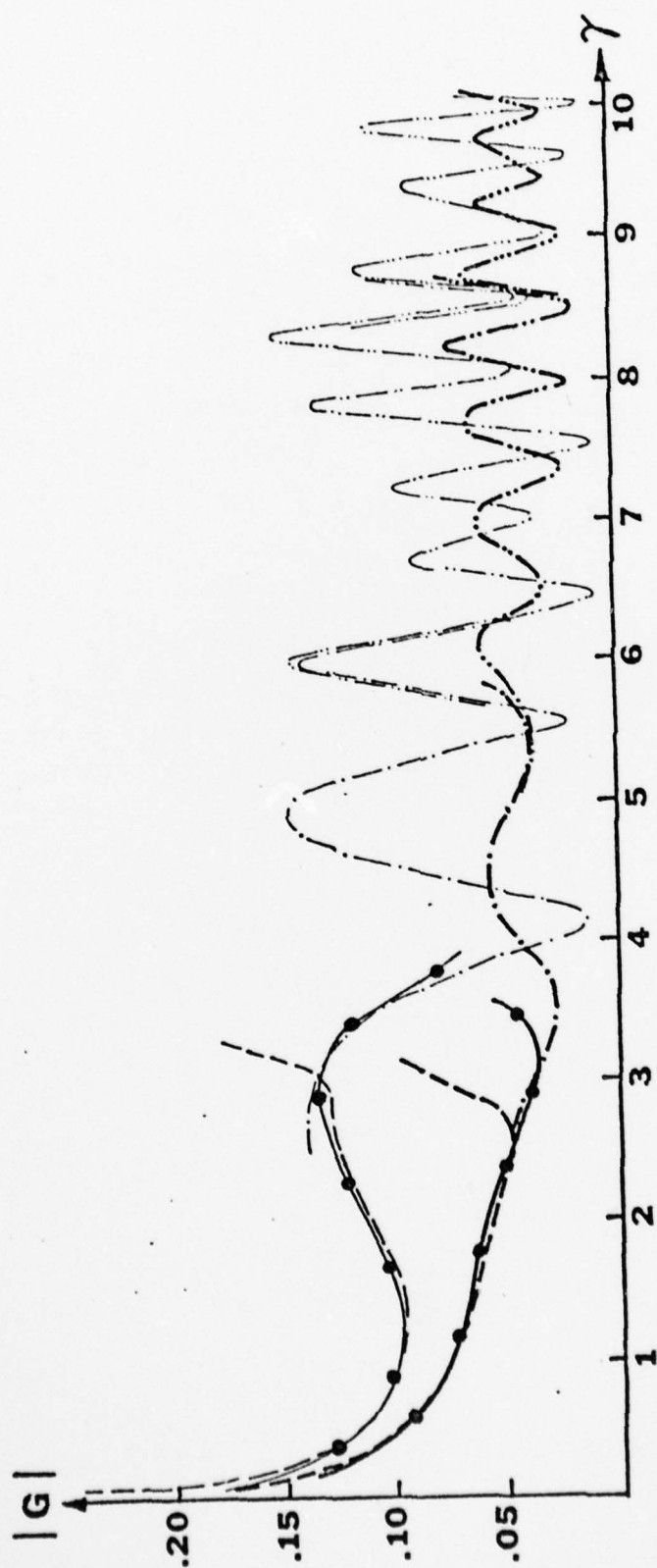
FIG. 9 (b)
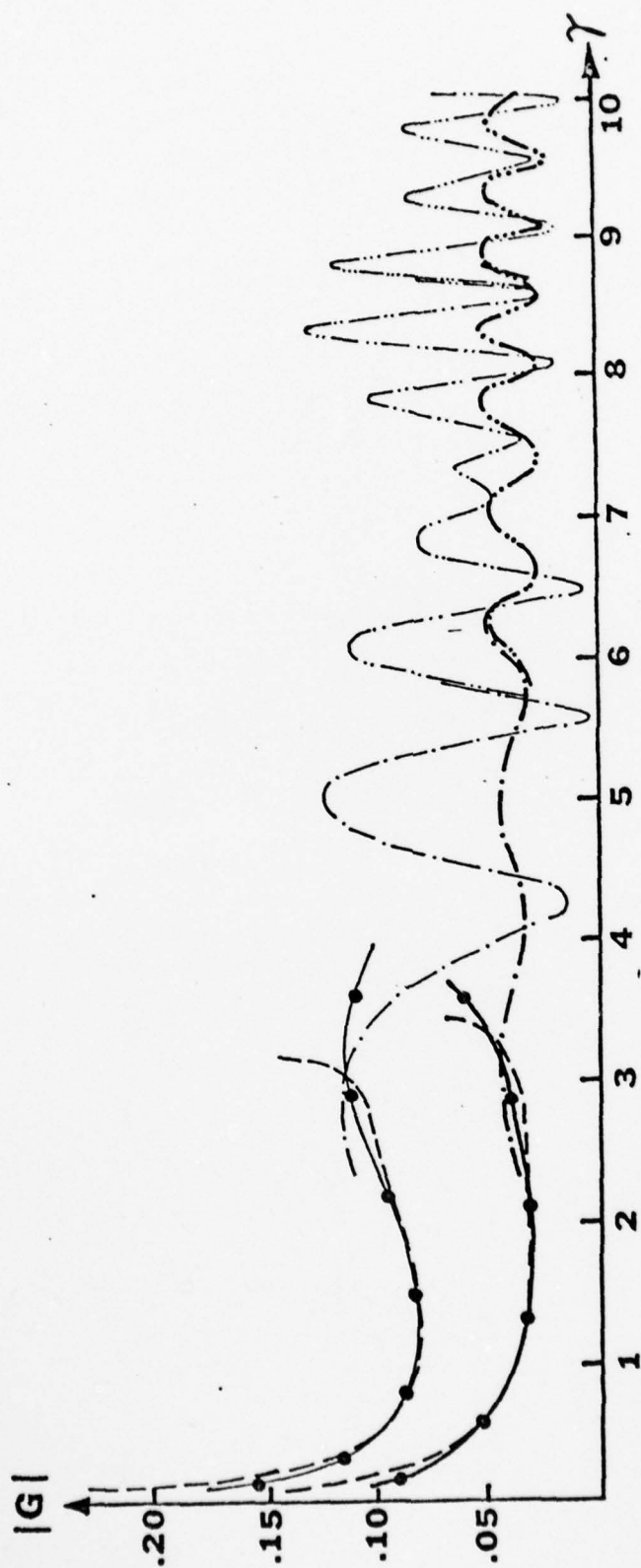
FIG. 9(c)
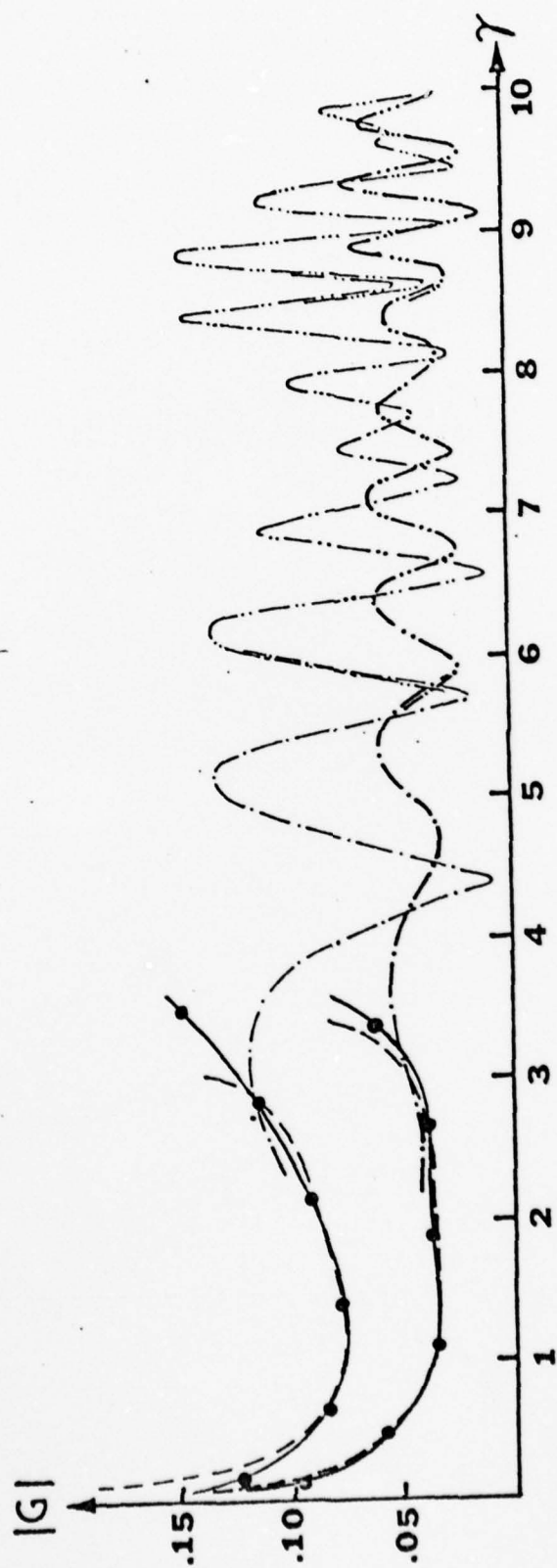
FIG. 9 (d)

FIG.9(e)

FIG.10 (a)

FIG.10 (b)

FIG.11